1971

The CO2 HN3~ laser: design and construction of a molecular laser pumped by photolysis of HN3.

Schnez, Gunther Paul.

Monterey, California ; Naval Postgraduate School

THE CO_2-HN_3 LASER: DESIGN AND CONSTRUCTION OF A MOLECULAR LASER PUMPED BY PHOTOLYSIS OF HN_3

Gunther Paul Schnez

United States
Naval Postgraduate School

THESIS

THE CO_2-HN_3 LASER:

DESIGN AND CONSTRUCTION OF A

MOLECULAR LASER PUMPED BY PHOTOLYSIS OF HN_3

by

Gunther Paul Schnez

Thesis Advisor: D.J. Collins

Approved for public release; distribution unlimited.

The CO_2-HN_3 Laser:

Design and Construction of a

Molecular Laser Pumped by Photolysis of HN_3

by

Gunther Paul Schnez
Lieutenant Commander, Federal German Navy
B.S., Naval Postgraduate School, 1970

Submitted in partial fulfillment of the
requirements for the degree of

MASTER OF SCIENCE IN ELECTRICAL ENGINEERING

from the

NAVAL POSTGRADUATE SCHOOL
June 1971

ABSTRACT

A CO_2-HN_3 laser is designed and constructed. The use of hydrazoic acid, being highly explosive and toxic, requires a design where the gas handling and optical systems are located inside a fume hood with exhaust to the outside. The laser utilizes a pumping scheme where energy released by the photolysis of HN_3 is used to create a population inversion in CO_2.

The major highlights of the developmental work are: (1) design and fabrication of the laser tube and resonant cavity, (2) design, construction and operation of the HN_3 generating and gas filling systems, and (3) flashlamp discharge circuit design and development of the charging control system.

Operation of the laser is the subject of subsequent work with the system. Preliminary experiments and suggestions are included in this study. Furthermore the basic principles and equations governing the operation of a CO_2-HN_3 laser are derived.

TABLE OF CONTENTS

I. HISTORY ---------- 8

II. THE LASING MECHANISM IN CARBON DIOXIDE -------- 11

A. CO_2-N_2 VIBRATIONAL-ROTATIONAL STATES ------ 11

B. POPULATION DISTRIBUTION IN THE CO_2-N_2 LASER 14

C. GAIN ---------- 21

III. THE HN_3-CO_2 LASER SYSTEM ---------- 27

IV. EXPERIMENTAL TECHNIQUES ---------- 30

A. GENERAL DESCRIPTION ---------- 30

B. HN_3 GENERATING SYSTEM ---------- 32

C. VACUUM SYSTEM ---------- 33

D. FLASHLAMP DRIVING CIRCUIT ---------- 36

E. ELECTRICAL SYSTEM ---------- 40

1. Charging System ---------- 40

2. Charging Control System ---------- 41

3. Trigger Circuit ---------- 42

4. Gas Handling Control System ---------- 42

F. OPTICAL SYSTEM ---------- 43

V. EXPERIMENTAL RESULTS ---------- 47

A. PRELIMINARY EXPERIMENTS ---------- 47

1. Operation of the Charging and Triggering System ---------- 47

2. Operation of the IR Detector and Photomultiplier ---------- 47

3. Operation of the Discharge Circuit ---- 49

4. Operation of the Vacuum System -------- 50

VI. SUMMARY ---------- 52

APPENDIX A: VIBRATIONAL RELAXATION TIMES ---------- 54

APPENDIX B: OPERATION OF THE GAS HANDLING SYSTEM ---- 56

APPENDIX C: FLASHLAMP DRIVING CIRCUIT PARAMETERS ---- 58

APPENDIX D: STABILITY REQUIREMENTS FOR CONFOCAL RESONATOR ---------- 62

APPENDIX E: ALIGNMENT PROCEDURE FOR THE OPTICAL SYSTEM ---------- 64

APPENDIX F: DRAWINGS ---------- 65

APPENDIX G: PHOTOGRAPHS ---------- 83

BIBLIOGRAPHY ---------- 90

INITIAL DISTRIBUTION LIST ---------- 92

FORM DD 1473 ---------- 93

LIST OF FIGURES

1. Vibrational States in the CO_2 Molecule ---------- 65

2. Pertinent Vibrational Energy Levels of CO_2 and N_2 66

3. Rotational Transitions of the (00°1) → (10°0) Band in CO_2 ---------- 67

4. Rotational Energy Levels of the (00°1) Vibrational State of CO_2 ---------- 67

5. Vibrational Energy Levels for the Simplified Model 68

6. Gain Coefficient as Function of Frequency -------- 69

7. Flash Input and Lasing Output Intensities in CO_2-HN_3 Laser ---------- 69

8. Experimental Setup ---------- 70

9. HN_3 Generating System ---------- 71

10. Vacuum System ---------- 72

11. Flashlamp Discharge Circuit ---------- 73

12. Normalized Flashlamp Current ---------- 74

13. Normalized Flashlamp Energy ---------- 74

14. Block Diagram of Charging System ---------- 75

15. Charging Control System ---------- 76

16. Flashlamp Trigger Circuit ---------- 77

17. Circuit Diagram for Gas Handling Control System -- 78

18. Optical System ---------- 79

19. Schematic of Setup for Grinding of Correct Angles on the Laser Tube Ends ---------- 79

20. Biasing Circuit for IR Detector ---------- 80

21. Lamp Lifetime vs. Energy Dissipated ---------- 81

22. Flash Energy vs. Capacitor Voltage ---------- 82

23. CO_2-HN_3 Laser and Control Panel ---------- 83

24. Optical Bench with Laser Flashlamp and IR Detector ---------- 84

25. HN_3 Generating Unit ---------- 85

26. High Voltage Power Supply with Capacitor Bank, Trigger Unit, and Oscilloscope ---------- 86

27. Distorted Flashlamp Output Detected by Photomultiplier and IR Detector ---------- 87

28. Flashlamp Output Detected by IR Detector and Discharge Current Pulse ---------- 87

29. Distorted Flashlamp Output Detected by IR Detector ---------- 88

30. Capacitor Voltage During Discharge ---------- 88

31. Capacitor Voltage and Discharge Current Pulse --- 89

ACKNOWLEDGEMENTS

The author wishes to express his gratitude to Professor Daniel J. Collins for his advice, encouragement and guidance. Professor Collins has been most generous in giving counsel where the material was unfamiliar and in supporting this project and its realization.

The author is deeply indebted to the staff of the Aeronautical, Electrical Engineering, Chemistry, and Physics Departments for providing facilities and technical assistance for this experimental work. A special note of appreciation is extended to Norman E. Leckenby, who gave of his time and effort to make this project a success; to Robert C. Scheile for his glassblowing skill and his knowledge of vacuum technology; and to Robert C. Smith for his able technical assistance in the design of the electrical system.

I. HISTORY

The Nobel Prize in Physics 1964, awarded to C.H. Townes, N.G. Basov, and A.M. Prokhorov, was the climax of public recognition of a most remarkable, if not revolutionary scientific discovery: the maser, ancestor of the laser.

The roots for this discovery go back to the early days of quantum physics when Einstein first introduced the idea of stimulated emission of radiation [Ref.1]. In the following years several scientists touched the idea of "negative absorption" and "stimulated emission," however, no proposals were made to make use of this radiation for amplifiers or oscillators.

After 1945, independent progress was made by a number of scientists toward the development of devices using stimulated emission in the microwave frequency range.

Late in 1953, Townes, then at Columbia University, New York, and his two research students, Gordon and Zeiger, succeeded in the operation of the first maser using ammonia molecules. In 1954, Basov and Prokhorov of the Lebedev Institute in Moscow, independently of Townes, designed and published a proposal for a very similar ammonia maser [Ref.2].

Once the feasibility of the maser had been demonstrated research concentrated on the development of masers at frequencies higher than the microwave region. Townes and

Dr. Arthur Schawlow from Bell Telephone Laboratories at Murray Hill, New Jersey, together proposed an optical maser using excited potassium vapor with a predicted wavelength of 3.14 microns, in the near infrared [Ref.2]. However, the system could not be made to work. In September 1959, during the first symposium on quantum electronics at Schawanga Lodge, High View, New York, Schawlow outlined a scheme for solid state optical masers using, for example, transitions in ruby. In July 1960, T.H. Maiman of the Hughes Aircraft Company's research laboratories at Malibu, California, who had been working with ruby illuminated by flashes of light, announced the successful operation of the first optical maser. In the same year, the term "Laser" was introduced to replace "Optical Maser" [Refs.2,3].

The first gas laser was built by A. Javan at the Bell Telephone Laboratories in the fall of 1960. Laser action occurred in a mixture of helium and neon utilizing transitions between electronic energy levels of the neon. By 1964, thirty-two gas combinations were known to produce laser emissions [Ref.4]. All of these systems, however, were inherently restricted to milliwatt outputs.

In the spring of 1964 C.K.N. Patel [Ref.5] published the discovery of a new type of laser: the molecular gas laser. His work with the CO_2 molecular laser opened the field for a new dimension in laser research and applications, created by the possibility of obtaining power outputs of several

watts. The work reported herein describes the design and construction of a variation of this basic CO_2 laser.

II. THE LASING MECHANISM IN CARBON DIOXIDE

A. CO_2-N_2 VIBRATIONAL-ROTATIONAL STATES

Every laser is a quantum mechanical device. Particles emit quanta of energy in the form of radiation that are released by transitions from higher to lower energy levels. Before Patel developed the molecular gas laser in 1964, all then known two-component gas lasers utilized an energy transfer between electronic states of the two-component gases [Ref.6]. The first molecular gas laser oscillation also was obtained from electronic transitions of a number of diatomic gases. The CO_2 molecular laser, however, makes use of transitions between vibrational states within the same electronic level of the CO_2 molecule. Although only a quantum mechanical treatment can accurately describe the vibrational energy levels in CO_2, a classical model will provide a more easily visualized and satisfactory explanation. As illustrated in Figure 1, the vibrational state of the molecule is described by three quantum numbers, v_1, v_2, and v_3, and is usually written in the form $(v_1 v_2 v_3)$, where v_1 describes the number of vibrational quanta in the symmetric stretch mode, v_2 the number of vibrational quanta in the bending mode and v_3 the number of vibrational quanta in the asymmetric stretch mode. The bending mode, being two-fold degenerate, usually carries a superscript to indicate the degeneracy. The vibrational energies corresponding to

modes and combinations of modes can be represented in an energy level diagram. Pertinent parts of such a diagram are given in Figure 2.

In addition to the quantization into vibrational levels there exist a number of rotational levels for each of the vibrational states [Ref.7], characterized by the quantum number J. A change in J of ± 1 corresponds to a change in rotational angular momentum of ± $h/2\pi$, where h is Planck's constant. Due to the symmetry of the CO_2 molecule, certain J values are prohibited depending on the vibrational state of the molecule. In particular, for the vibrational levels utilized in a CO_2 laser at 10.6 microns, even J levels are absent in the upper laser level, (001), and odd J levels in the lower laser level, (100) [Ref.8]. Transitions between these two vibrational levels therefore result in a vibrational rotational band, where the center of the band corresponds to the spacing between the vibrational levels in the absence of any rotational energy (Figure 3). There are no transitions in the center of the band because ΔJ can not be zero for the levels involved. The allowed transitions corresponding to $\Delta J = +1$ are called P-branch transitions (longer wavelength), whereas those corresponding to $\Delta J = -1$ are called R-branch transitions (shorter wavelength). Figure 4 shows the Boltzmann distribution of the population densities of the rotational energy levels of the upper laser level. A similar distribution holds for the lower laser

level. The P-branch transition from the K = 21 level of the (001) state to the j = 22 level of the (100) vibrational state has the highest gain [Ref.7] and starts oscillating, thereby emitting radiation at 10.6 microns. Due to the very short relaxation time of the rotational levels ($\approx 10^{-7}$ sec), the original Boltzmann distribution is maintained by transfer of molecules from other rotational levels to the J = 21 level. Thus the population density of all the rotational levels decreases even though laser oscillation keeps drawing the molecules from the J = 21 level. As a result the output of a CO_2 laser occurs predominantly on a single rotational transition of the $(00^{\circ}1) \rightarrow (10^{\circ}0)$ band, thereby ensuring very coherent and monochromatic radiation at 10.6 μm. Similarly, lasing at 9.6 μm results from a single rotational transition of the $(00^{\circ}1) \rightarrow (02^{\circ}0)$ band. However, since the intensity of radiation at this shorter wavelength is only 1/10 that at 10.6 μm [Ref.7], the following analysis will consider the $(00^{\circ}1) \rightarrow (10^{\circ}0)$ vibrational transition only. In Figure 2 the rotational levels have not been shown for simplicity. The indicated wavelengths correspond to the dominating transition within the vibrational-rotational band.

The addition of nitrogen to a CO_2 laser results in the selective excitation of the CO_2 molecules to the upper laser level. Nitrogen, a diatomic molecule, has only one degree of vibrational freedom described by the quantum number v.

Since the energies of the excited $N_2(v=1)$ and $CO_2(00°1)$ are almost equal (this holds also for the higher energy levels), an efficient transfer of vibrational energy through collisions between the excited states of $N_2(v = 1, 2, 3,...)$ and the corresponding levels of the asymmetric stretch mode of CO_2 is possible. Moreover, in N_2 and CO_2 these excited levels are approximately evenly spaced [Ref.7]. This allows a redistribution of vibrational energy between molecules in higher excited states and those in the ground state, exciting them to $N_2(v = 1)$ and $CO_2(00°1)$ respectively. It is this transfer of vibrational energy through collisions that is utilized in the excitation of virtually every CO_2 laser.

B. POPULATION DISTRIBUTION IN THE CO_2-N_2 LASER

At thermal equilibrium the CO_2 molecules are distributed among the allowed energy levels according to the Boltzmann distribution:

$$\frac{N_n}{N_m} = \frac{g_n}{g_m} \, e^{-\frac{(E_n - E_m)}{KT}} \qquad (2\text{-}1)$$

where

N_n, N_m = number of molecules per unit volume in the n^{th}, m^{th} state

E_n, E_m = vibrational energy in the n^{th}, m^{th} state

g_n, g_m = statistical weight of the n^{th}, m^{th} state

n, m = 0, 1, 2, 3...

K = Boltzmann constant

T = absolute temperature

and

$$N_0 + N_1 + N_2 + N_3 + \ldots = N \qquad (2\text{-}2)$$

where

N = total number of molecules per unit volume.

From Equation (2-1) it follows that at T = 0, all molecules are in the ground state. At T > 0 thermal equilibrium requires that a state with lower energy be more densely populated than a state with higher energy. In order to allow laser action the equilibrium condition must be disturbed by an inversion of population density between at least one pair of allowed energy levels. In such a system the higher energy level is also the more densely populated. To simplify the calculation of population densities in a CO_2-N_2 laser system the Boltzmann relation may also be used to describe the participating vibrational energy levels in the non-equilibrium condition of an inverted population [Refs.9, 10, 11]. If this is done, the temperature in Equation (2-1) becomes an effective temperature, T_i, that is characteristic for the excitation of each vibrational temperature T.

Another important simplification can be made by using the results of a survey of data by Taylor and Bitterman [Ref.12]. Their study shows an extremely fast vibrational resonant energy transfer between the N_2(v=1) and CO_2(00°1)

levels, as well as a very fast energy exchange between $CO_2(10°0)$ and $CO_2(02°0)$ due to Fermi resonance. In addition, because of the nearly equal spacing of the bending mode (v_2) of CO_2, vibrational energy is rapidly transferred to the $CO_2(010)$ level. A similar argument holds for the higher excited levels of $CO_2(00°v_3)$ and N_2.

The simplifying assumptions made above allow the construction of the following three-level approximation for the CO_2 laser [Refs.11, 13].

Mode 0 - ground state, no vibrational excitation

Mode I - excited states in the symmetric stretching and bending modes of CO_2

Mode II - excited states in N_2 and the asymmetric stretching mode of CO_2.

The modes are in thermal equilibrium within themselves, but not with each other. In each mode the Boltzmann distribution is established with its characteristic vibrational temperature T_i. As a result, the set of rate equations for the populations of all possible vibrational levels can now be replaced by a few balance equations for the simplified model. This approach is valid as long as the rate of energy transfer within each mode is much faster than the energy exchange rate between modes. A schematic of the grouping of energy levels for the simplified model is given in Figure 5.

For the following calculations it will be assumed that the modes can be approximated as harmonic oscillators [Ref.14]. Their energies are then given by

$$\frac{d}{dt} E_1 = \frac{1}{\tau_1} (E_{1e} - E_1) \qquad (2\text{-}3)$$

and

$$\frac{d}{dt} E_2 = \frac{1}{\tau_2} (E_{2e} - E_2) \qquad (2\text{-}4)$$

where

E_1, E_2 = net vibrational energy contained in mode I, II at the vibrational temperature T_1, T_2,

E_{1e}, E_{2e} = equilibrium vibrational energy contained in mode I, II at the local gas translational temperature, T

τ_1, τ_2 = characteristic relaxation time for mode I,II.

The relaxation times τ_1 and τ_2 are averages which characterize the net rate of energy transfer between the modes in the simplified model. The three major transitions in this model will be defined as follows:

(1) transition "a" between modes I and II with relaxation time τ_a

(2) transition "b" between modes 0 and II with relaxation time τ_b

(3) transition "c" between modes 0 and I with relaxation time τ_c.

The relaxation times τ_a, τ_b, and τ_c are determined by the CO_2-CO_2, CO_2-N_2, and N_2-N_2 collisions. They can be visualized as "resistances," where the total relaxation time of the gas mixture is equal to the "parallel resistance" of the relaxation times of its components, or

$$\frac{1}{\tau_a} = X_{CO_2} \frac{1}{\tau_a(CO_2\text{-}CO_2)} + X_{N_2} \frac{1}{\tau_a(CO_2\text{-}N_2)} \qquad (2\text{-}5)$$

where X_{CO_2} and X_{N_2} denote the mole fractions of CO_2 and N_2 present in the mixture. Similar expressions hold for τ_b and τ_c. The values of the component relaxation times, $\tau_a(CO_2\text{-}CO_2)$, etc., depend on the transition probability of participating levels, gas pressure, and temperature. Data are given in Appendix A.

It may be noted that the general quantity τ can be interpreted as a mean time required for a single particle to make a transition from one state to another state due to collisions with other particles. Hence $1/\tau$ represents the number of transitions of one particle per second. Thus the physical meaning of Equation (2-5) can be stated as follows: The total number of particle transitions per second due to collisions in the mixture is equal to the sum of particle transition due to collisions with each species present in the mixture. A similar physical representation can be given to the

average relaxation times of modes I and II. Making use of the "parallel resistance rule" again, they are given by

$$\frac{1}{\tau_1} = \frac{1}{\tau_c} \tag{2-6}$$

$$\frac{1}{\tau_2} = \left[\frac{X_{CO_2}}{\tau_a} + \frac{X_{N_2}}{\tau_b} \right] \frac{1}{X_{CO_2} + X_{N_2}} \tag{2-7}$$

Equations (2-6) and (2-7) are combined with Equations (2-3) and (2-4) to calculate E_1 and E_2 where E_{1e} and E_{2e} are defined by the following equilibrium relations

$$E_{1e} = m_C R_C \left[\frac{\frac{h\nu_1}{K}}{e^{\frac{h\nu_1}{KT}} - 1} + \frac{2\,\frac{h\nu_2}{K}}{e^{\frac{h\nu_2}{KT}} - 1} \right] \tag{2-8}$$

$$E_{2e} = m_C R_C \left[\frac{\frac{h\nu_3}{K}}{e^{\frac{h\nu_3}{KT}} - 1} \right] + m_N R_N \left[\frac{\frac{h\nu}{K}}{e^{\frac{h\nu}{KT}} - 1} \right] \tag{2-9}$$

where

m_C = mass fraction of CO_2

R_C = specific gas constant for CO_2

m_N = mass fraction of N_2

R_N = specific gas constant for N_2

ν_1, ν_2, ν_3 = characteristic vibrational frequencies of the symmetric stretching, bending, and asymmetric stretching mode respectively

ν = vibration frequency of N_2

T = translational temperature.

In Equation (2-8) the degeneracy of the bending mode has been taken into account by doubling its energy.

In a non-equilibrium situation the vibrational temperatures for mode I and II, T_1 and T_2, are defined by relations similar to Equations (2-8) and (2-9):

$$E_1 = m_C R_C \left[\frac{\frac{h\nu_1}{K}}{e^{\frac{h\nu_1}{KT_1}} - 1} + \frac{2\,\frac{h\nu_2}{K}}{e^{\frac{h\nu_2}{KT_1}} - 1} \right] \qquad (2\text{-}10)$$

$$E_2 = m_C R_C \left[\frac{\frac{h\nu_3}{K}}{e^{\frac{h\nu_3}{KT_2}} - 1} \right] + m_N R_N \left[\frac{\frac{h\nu}{K}}{e^{\frac{h\nu}{KT_2}} - 1} \right] \qquad (2\text{-}11)$$

Knowing the vibrational temperature of the energy levels within modes I and II, their population can be computed assuming a Boltzmann distribution locally within each mode. For example, the population of the (001) level in CO_2 is obtained from

$$N_{001} = \frac{N_{CO_2}}{Q}\, e^{-\frac{h\nu_3}{KT_2}} \qquad (2\text{-}12)$$

where N_{CO_2} is the number of molecules of CO_2 per unit volume and

$$Q = \left(1-e^{\frac{-h\nu_1}{KT_1}}\right)^{-1}\left(1-e^{\frac{-h\nu_2}{KT_1}}\right)^{-2}\left(1-e^{\frac{-h\nu_3}{KT_2}}\right)^{-1} \qquad (2\text{-}13)$$

is the partition function.

Similarly,

$$N_{100} = \frac{N_{CO_2}}{Q}\ e^{-\frac{h\nu_1}{KT_1}} \qquad (2\text{-}14)$$

C. GAIN

So far only one of the conditions for lasing action, namely population inversion as a requirement for stimulated emission, has been considered. Another, equally important factor is the amplification of the emitted radiation in an optical resonator. For lasing to take place it is required that the gain be great enough to surpass the inevitable resonator losses. If f is the fractional loss per pass, then the condition needed is [Ref.15]

$$f < \frac{I-I_0}{I} \qquad (2\text{-}15)$$

where I_0 and I are light intensities before and after passage through the amplifying material and are related by

$$I = I_0\ e^{-Kx} \qquad (2\text{-}16)$$

for propagation in the x direction. K is the absorption coefficient of the material,

$$\left.\begin{aligned} Kx &= -\ln \frac{I}{I_0} \\ K &= -\frac{1}{I}\frac{dI}{dx} \end{aligned}\right\} \qquad (2\text{-}17)$$

For a certain frequency ν the rate of change of radiation intensity, $dI(\nu)$, as it propagates in a gas along the x axis is governed by the simultaneous process of spontaneous emission, stimulated emission, and absorption.

For light of frequency between ν and $\nu+d\nu$ the increase of energy in the beam is given by [Ref.16]:

$$d[I(\nu)d\nu] = \frac{h\nu}{4\pi}[A_{21}dN_2(\nu)+B_{21}I(\nu)dN_2(\nu)-B_{12}I(\nu)dN_1(\nu)]dx \qquad (2\text{-}18)$$

where A_{21}, B_{21}, B_{12} are the Einstein coefficients for spontaneous emission, induced emission, and absorption; $dN_1(\nu)$ and $dN_2(\nu)$ are the numbers of absorbers and emitters in the lower and upper laser levels; c is the velocity of light in the laser medium.

Equation (2-18) can be simplified by making use of the fact that spontaneous emission is non-directional and does therefore not contribute significantly to laser action, as compared with induced emission which is coherent with the stimulating radiation and therefore reinforces the beam.

$$\left[\frac{1}{I(\nu)}\frac{dI(\nu)}{dx}\right]d\nu = \frac{h\nu}{4\pi}[B_{21}dN_2(\nu)-B_{12}dN_1(\nu)] \qquad (2\text{-}19)$$

Using Equation (2-17) and integrating over the entire line centered around ν_0,

$$\int_0^\infty -K(\nu)d\nu = \frac{h\nu_0}{4\pi} (B_{21}N_2 - B_{12}N_1) \qquad (2\text{-}20)$$

where N_1 and N_2 are the numbers per unit volume of all absorbers and emitters on the transition of center frequency ν_0. From Planck's radiation law and assuming a Boltzmann distribution under equilibrium conditions, the following relations can be derived [Refs.16,17]:

$$\left.\begin{aligned} g_1 B_{12} &= g_2 B_{21} \\ B_{21} &= \frac{c^2}{2h\nu^3} A_{21} \end{aligned}\right\} \qquad (2\text{-}21)$$

where g_1 and g_2 are the degeneracies of the lower and upper laser levels. It should be noted at this point that the B coefficients have been defined in terms of intensity of isotropic radiation, $I(\nu)/4\pi$ (see also Equation (2-18)), whereas the original Einstein B coefficients were defined in terms of radiation density. The two kinds of B's are related by

$$B(\text{density}) = \frac{c}{4\pi} B(\text{intensity}) \qquad (2\text{-}22)$$

Also, from Ref.16,

$$A_{21} = \frac{1}{\tau_{21}} \qquad (2\text{-}23)$$

where τ is the radiative lifetime of the atom. Substituting Equation (2-21) into (2-20) results in

$$\int_0^\infty \alpha(\nu)d\nu = S(\nu_0) = \frac{c^2 A_{21} g_2}{8\pi\nu_0^2 g_1}\left(\frac{g_1}{g_2}\ N_2 - N_1\right) \qquad (2\text{-}24)$$

where the negative absorption coefficient $K(\nu)$ has been redefined as gain coefficient $\alpha(\nu)$ and $S(\nu_0)$ is the line strength. A graph of $\alpha(\nu)$ vs. ν is given in Figure 6. Here the line width is defined to be given by $\Delta\nu$, the width of the emitted line at half maximum. The exact shape of the curve in Figure 6 may vary depending upon which physical principle is the dominating cause for line broadening in a given situation. The two major effects to be considered are Doppler broadening and collision broadening. At higher temperatures or lower pressures the optical transitions in a gas are broadened principally by Doppler shifts due to thermal motion in the gas [Ref.15]. The result is a Gaussian line shape with a $\Delta\nu$ of

$$\Delta\nu = \frac{2\nu_0}{c}\left(\frac{2KT}{m}\ln 2\right)^{1/2} \qquad (2\text{-}25)$$

where K = Boltzmann constant

T = absolute temperature

m = mass of molecule.

At higher pressures and lower temperatures, the intermolecular collisions significantly reduce the length of

time that the quantum state of a molecule is unperturbed [Ref. 15]. Collision broadening becomes important, resulting in a Lorentzian line shape with $\Delta\nu$ defined by

$$g(\nu) = \frac{\Delta\nu}{2\pi} \frac{1}{(\nu-\nu_0)^2 + \left(\frac{\Delta\nu}{2}\right)^2} \tag{2-26}$$

At line center,

$$\Delta\nu = \frac{2}{\pi} \frac{1}{g(\nu_0)} \tag{2-27}$$

where $g(\nu_0)$ is a line shape factor [Ref.17] given by

$$g(\nu_0) = \frac{2}{\sum_i N_i \sigma_i \left[\frac{8RT}{\pi}\left(\frac{M_{CO_2} + M_i}{M_{CO_2} M_i}\right)\right]^{1/2}} \tag{2-28}$$

Here N_i = number of molecules per unit volume of species i

σ_i = collision cross-section for collisions between CO_2 and species i

M_{CO_2} = molecular weight of CO_2

M_i = molecular weight of species i

R = universal gas constant.

The gain coefficient for collision broadening is, from Ref.15,

$$\alpha(\nu) = \frac{S(\nu_0)}{2\pi} \frac{\Delta\nu}{(\nu-\nu_0)^2 + \left(\frac{\Delta\nu}{2}\right)^2} \tag{2-29}$$

The gain α_0 at the center of the line becomes, substituting Equation (2-24)

$$\alpha_0 = \frac{2}{\pi\Delta\nu} \frac{c^2 A_{21} g_2}{8\pi\nu_0^2 g_1} \left(\frac{g_1}{g_2} N_2 - N_1 \right) \tag{2-30}$$

At pressures above 10 torr the line width is, from Ref.17, predominantly collision broadened. For the CO_2 laser transition between levels (001) and (100), with $g_1 = g_2 = 1$, the gain can finally be written, making use of Equation (2-27),

$$\alpha_0 = \frac{\lambda^2}{8\pi} A_{001-100} \left(N_{001} - N_{100} \right) g(\nu_0) \tag{2-31}$$

where λ is the wavelength at center line and $g(\nu_0)$ is as defined by Equation (2-28). The following data are given in Ref.17:

$$A_{001-100} = \frac{1}{\tau_{21}} = \frac{1}{5.38 \text{ sec}} = 0.186 \ (\text{sec}^{-1})$$

$$\sigma_{CO_2} = 1.30 \times 10^{-14} \ (\text{cm}^2)$$

$$\sigma_{N_2} = 0.87 \times 10^{-14} \ (\text{cm}^2)$$

$$\sigma_{He} = 0.37 \times 10^{-14} \ (\text{cm}^2)$$

III. THE HN_3-CO_2 LASER SYSTEM

In the previous section a CO_2 laser scheme has been investigated in which the upper laser level was pumped predominantly by vibrational energy transfer from excited nitrogen. An obvious way to increase the laser efficiency is to find a pumping scheme where ideally all or at least a large fraction of the N_2 molecules could be raised to an excited energy state. One method of achieving this was found by Basov [Ref.18] who in July 1969 reported the successful operation of a chemically pumped laser. In this experiment Basov obtained population inversion within the energy levels of CO_2 by flash photolysis of a mixture of hydrazoic acid (HN_3) and carbon dioxide where the decomposition of HN_3 produced nitrogen molecules in an excited state. A very similar experiment has been carried out by Dzhidzhoev and co-workers; it is described in detail in Ref.19. In this work only the highlights of the CO_2-HN_3 laser will be presented.

The mechanism of the photolysis reaction is principally determined by the following processes [Refs.18,19]:

$$HN_3 + h\nu \rightleftarrows NH^* + N_2 - 10 \text{ Kcal} \qquad (3\text{-}1)$$

$$NH^* + HN_3 \rightleftarrows H_2 + N_2 + N_2^* + 152 \text{ Kcal} \qquad (3\text{-}2)$$

$$N_2^* + \alpha HN_3 \rightleftarrows \alpha N_2^* + \alpha NH^* + N_2 \qquad (3\text{-}3)$$

$$N_2^* + M \rightleftarrows N_2 + M^* \qquad (3\text{-}4)$$

$$M + HN^* \rightleftarrows M^* + HN \qquad (3\text{-}5)$$

Here HN* and N_2* are vibrationally excited molecules. M is a diluent molecule, and α is the average number of HN_3 molecules activated by one N_2* molecule.

The equations above form a chain reaction with the chain branched for $\alpha > 1$. Rate constants are not available, however it can be assumed that the reaction is fast compared to the rate of transfer of vibrational energy to other degrees of freedom [Ref.19]. This is important since lasing can only be expected if the pumping rate exceeds the relaxation rate as defined by Equation (2-5). In Figure 7 a graph showing relative intensity vs. time of the triggering light flash and the resulting lasing action is given as obtained by Basov [Ref.18] with a resonator of 1.5 m length and 30 mm diameter.

For the energy and gain calculations of the CO_2-HN_3 laser the results obtained previously for the CO_2-N_2 laser can be used with a slight modification. For the low pressures of a few torr typically employed for CO_2-N_2 lasers [Refs.20,21], the modes in Figure 5 had been approximated as harmonic oscillators that were assumed to relax independently of each other. This is no longer valid at the higher pressures used in the CO_2-HN_3 laser, typically 50 to 100 torr. For this case energy from mode II is fed into Mode I with the result that the lower energy level can no longer relax independently of the upper level. The energy E_1 of mode I as given by Equation (2-3) will therefore have to be

redefined such that the energy feeding from mode II is included. A treatment of this problem is given in Ref.22.

The gain of the CO_2-HN_3 laser is, for a predominantly collision broadened line, given by Equation (2-31). Unknown in this relation are the populations of the upper and lower laser levels of CO_2. According to Ref.19 the energy obtained by the decomposition of HN_3 into nitrogen and hydrogen is 71 Kcal/mole and it may be assumed that most of this energy is transferred into the vibrational energy of the nitrogen molecules. However, without knowing the rate constants in Equations (3-1) through (3-5), the number of molecules in vibrationally excited states of CO_2 can not be calculated.

An alternative method to obtain a measure of population inversion for the CO_2-HN_3 laser is indicated in Ref.19. The investigation of the infrared spectrum of CO_2 emission leads to a measure of the vibrational temperatures in modes I and II as defined above. From Equations (2-12) and (2-14) the number of CO_2 molecules in the upper and lower laser levels can now be computed. The gain calculation for the CO_2-HN_3 laser is then carried out as described in Chapter II-A. A design for this laser is given in the following chapter.

The flashlamp is a linear xenon-filled quartz tube mounted parallel to the laser tube at a distance of about 1.5 cm. To intensify the light flash and ensure fast and simultaneous initiation of the photolysis reaction over the entire length of the laser both tubes are enclosed by a common cylindrical metal shell lined with highly reflecting aluminum foil.

To detect the laser output at 10.6 microns a gold doped germanium infrared detector is used, operated at 77°K (liquid nitrogen temperature). The output is amplified and made visible on a dual beam oscilloscope. The other beam simultaneously shows the input from the flashlamp using a photo diode.

The laser is operated at room temperature. The temperature inside the fume hood is normally raised a few degrees using a 100 W light bulb to minimize deterioration of the sodium chloride laser windows.

The experiment consists of the following basic steps:

1. The HN_3 generating apparatus is set up with measured amounts of reagents ready for mixing.

2. The capacitor bank is charged to desired voltage.

3. Generation of HN_3 is started and the evacuated system is filled with predetermined amounts of HN_3, CO_2, and any additional gases.

4. The laser is ready for one-shot operation. Photolysis is started by firing of flashlamp.

5. Lasing action occurs and is recorded on oscilloscope.

B. HN_3 GENERATING SYSTEM

Hydrazoic acid (HN_3) is generated in a pyrex flask (Figure 9) using (1) NaN_3, sodium oxide (solid in powder form), and (2) H_3PO_4, phosphoric acid (syrupy solution in water, 80%). The amount of NaN_3 is measured accurately, mixed with mineral oil and placed into the generating flask by removing the relief valve assembly. The mineral oil considerably eases handling of the highly toxic and somewhat explosive NaN_3 powder and will not affect the experiment [Ref.23]. H_3PO_4 is added to obtain the following reaction:

$$NaN_3 + H_3PO_4 \rightarrow HN_3\ NaH_2PO_4 \qquad (4\text{-}1)$$

Knowing the volume of the vacuum system the necessary amount of NaN_3 can be calculated to obtain any desired partial pressure of HN_3. The quantity of H_3PO_4 used in the generation of HN_3 is chosen slightly higher than required by Equation (4-1) to ensure complete reaction of NaN_3. Like the mineral oil, the excess phosphoric acid does not interfere with the experiment [Ref.23] and will be neglected. A magnetic stir (with teflon covering) is used to keep the reagents thoroughly mixed.

The generated HN_3 is then brought into the stainless steel manifold through a combination of two ball joints and a flexible connection (bellows). This arrangement provides a fast and easy way to disconnect the generating unit from

the manifold after each experiment for cleaning purposes and also ensures a reliable vacuum seal after replacement.

The measuring of the NaN_3 is done by weighing an amount in a small glass jar of known weight. The filling of the jar and necessary adjustments are made inside the fume hood to avoid accidental breathing of the powder. During the procedure the sliding window is opened just enough to reach inside the hood.

H_3PO_4 is measured by manually opening stopcock M1 slightly while the system is evacuated. The desired amount can be read from a mm^3 scale as shown in Figure 9. M2 is kept closed during measuring to avoid accidental spilling into the generating flask. After closing the sliding window, generation of HN_3 is started by opening A with a reversible AC motor. The motor turns the stopcock 90° in 15 seconds with an automatic stop in the open and closed position. A relief valve opens to the exhaust at atmospheric pressure to prevent damage from possible overpressure in the generating unit. The valve is also used during flushing of the system.

A procedure for the operation of the generating system as part of the gas handling system is given in Appendix B.

C. VACUUM SYSTEM

The design of the vacuum system was determined by the following requirements:

1. To provide a specified mixture of gases to the laser tube.

2. It must consist of non-corrosive materials for handling of hydrazoic acid.

3. Location of those parts of the system exposed to HN_3 within the fume hood.

4. Operation of the system by remote control.

A schematic of the system is given in Figure 10. It consists of 1/4" stainless steel tubing and a 1/8" manifold. This allows the use of stainless steel valves that are operated by solenoids from a remote control panel. A mechanical vacuum pump is used able to produce a vacuum of 10^{-3} torr. Before each experiment the system is flushed with nitrogen, to eliminate unwanted gases. Nitrogen was chosen since it is also used as a component in the laser gas mixture and any remaining traces after pumping will therefore not affect the outcome of the experiment. A regulator between the nitrogen bottle and valve B is installed to provide constant pressure to the system and as a precaution against accidental overpressure.

The gases used in the laser are of research grade and come in 1 liter pyrex flasks at a pressure of 755 mm of mercury. Their guaranteed purity is:

CO_2: 99.995%

N_2: 99.999%

He: 99.9995%

The flasks are connected to the manifold using glass-to-metal seals. Each gas component employed in an experiment

is introduced into the system separately through valves S,C, N, and H. Since the solenoids do not allow gradual opening, needle valves with a preset flow rate are located immediately behind the inlets. Manually operated bypasses provide an easy way to adjust the rate of flow to a convenient value. This allows an accurate measurement of each gas component present by observing the absolute pressure in the system. The pressure is measured using a stainless steel Bourdon tube gauge with a range from 0 to 750 mm of mercury with a precision of 0.1% full scale. For more accurate readings at low pressures an additional thermocouple gauge is used.

The laser tube consists of fused quartz and is 60 cm long with 20 mm inner diameter. The ends are closed with sodium chloride Brewster windows that are glued to the laser tube ends with General Electric silicone rubber for an easy, inexpensive and effective seal. The laser tube is connected to the stainless steel tubing by a combination of ball joints and stainless bellows as shown in Figure 10. This has the twofold advantage of eliminating mechanical tension between the laser tube and the rest of the system and it makes the installation particularly simple.

A step-by-step procedure for the operation of the entire gas handling system is given in Appendix B.

D. FLASHLAMP DRIVING CURCUIT

The flashlamp driving circuit consists of two electrically isolated parts: The discharge circuit and the triggering network.

The discharge circuit has the following components:

1. An ILC model 10L24 xenon filled flashlamp, 60 cm by 10 mm, with a fused quartz envelope and nickel plated copper electrodes.

2. A capacitor bank consisting of four 7 μF and two 1.5 μF high voltage (up to 25 KV) capacitors in parallel.

3. An inductance made of 3/8 inch copper tubing with 25 windings and a diameter of 15 cm.

The components are put together in series as shown in Figure 11, using 3 x 1/4 inch copper bars and, inside the fume hood, 3/8 inch copper tubing. All connections are silver soldered to minimize losses. The remaining very small ohmic resistance (R = 0.0018 ohms) has been neglected in the circuit design. The effects will be considered later.

A calculation of the operating parameters is given in Appendix C. The most important single parameter, the pulse duration T, is determined by the values of C and L. Since variations in C are not easily obtainable due to the physical size of the capacitors, the desired pulse duration is specified by the inductance. It must be short enough to avoid overlapping with the beginning of laser action [Ref.18]. On the other hand, Markiewicz and Emmett [Ref.24] point out

that at total pulse lengths of less than 100 to 125 sec an additional arc inductance and hysteresis in the V-I-characteristic become important for flashlamps of the kind used.

For the range of operation in this study, the voltage-current characteristic of the flashlamp can be represented [Ref.24] as

$$v = \pm K_0 \mid i \mid^{1/2} \tag{4-2}$$

The sign is chosen to be the same as the sign of i. K_0 is the lamp impedance parameter and can be considered to be a nonlinear resistance with units (ohms - amps 1/2). K_0 is determined by

$$K_0 = k \frac{l}{d} \tag{4-3}$$

where

l = length of discharge column

d = diameter of discharge column

k = proportionality constant, dependent on gas mixture in the lamp.

For the flashlamp used K_0 is given by the manufacturer.

The flashlamp discharge curcuit shown in Figure 11 is described by the nonlinear differential equation:

$$L \frac{di}{dt} \pm K_0 \mid i \mid^{1/2} + \frac{1}{c} \int_0^t i \, d\tilde{t} = V \tag{4-4}$$

where V = voltage of the capacitor bank. This relationship can be simplified by making the following substitutions and normalizations:

$$\left.\begin{aligned} Z_0 &= \left(\frac{L}{C}\right)^{1/2} \\ i &= I\,\frac{V}{Z_0} \\ \tau &= (LC)^{1/2} \\ t' &= \frac{t}{\tau} \end{aligned}\right\} \qquad (4\text{-}5)$$

$$\alpha = \frac{K_0}{(VZ_0)^{1/2}} \qquad (4\text{-}6)$$

Equation (4-4) now becomes

$$\frac{dI}{dt'} \pm \alpha \mid I \mid^{1/2} + \int_0^{t'} I\, d\tilde{t}' = 1 \qquad (4\text{-}7)$$

where α is the damping parameter for the circuit. A solution of Equation (4-7) has been obtained by Markiewicz and Emmett using a digital computer. Using their results and the data calculated in Appendix C, a graph of I vs. t is given in Figure 12. The energy dissipated in the lamp is

$$E = \int_0^t P\, d\tilde{t} \qquad (4\text{-}8)$$

where the power P is given by

$$P = vi = K_0 \mid i \mid^{3/2} \tag{4-9}$$

A graph of E vs. t is given in Figure 13.

So far the effect of circuit loss has not been considered. A constant resistive loss R in the circuit will produce a term Ri in Equation (4-4), which will modify Equation (4-7) to become

$$\frac{dI_s}{dt'} \pm \left[\alpha + |I_s|^{1/2} \frac{R}{Z_0}\right] |I_s|^{1/2} + \int_0^{t'} I_s dt' = 1 \tag{4-10}$$

The energy dissipated by this linear loss is

$$E_R = R \int_0^{\infty} i_s^2 \, dt \tag{4-11}$$

Assuming that for very small R, i_s can be approximated by i as calculated for the lossless case, E_R can be estimated using Figure 12. For the given circuit parameters the loss is found to be within 1% of the energy supplied to the flashlamp and can be neglected in this case. It would increase, however, to about 10% if the resistive loss were only a little higher, like 0.04 ohms.

Another factor that might affect the flashlamp performance are the effects of short pulses mentioned earlier. Both hysteresis and arc inductance tend to produce a pulse that is more underdamped than would be expected. At the

short pulse duration selected for this experiment some of these effects may be present.

The triggering network essentially represents a switch in the discharge circuit that must be closed to dump the energy from the capacitor bank into the lamp. A description of the trigger circuit is given in the following section.

E. ELECTRICAL SYSTEM

The electrical system basically consists of the high voltage charging system for the capacitor bank, the charging control system, and the trigger circuit. The circuitry for the remote control operation of the gas handling system is also included in this section. A brief description of each of these basic elements is given below. The system has been designed and built nearly entirely from components available on campus. In particular, portions of the high voltage equipment used in earlier experiments ("exploding wire" and others) could be used directly or were modified for use in the charging system.

1. Charging System

A basic block diagram of the charging system is given in Figure 14. In the "dumped" condition the high voltage vacuum switches are in their normal (de-energized) position: switch 1 is open, switch 2 closed. In the "charging" condition the position of the vacuum switches is reversed and the capacitor bank is charged in series with a 3 MΩ resistor by a NJE (New Jersey Electronics) Model HA-51 variable

high voltage power supply (0-30 KV 0-10μA). The charging current can be read from an ampere meter in the power supply panel (not shown in Figure 14).

The voltage on the capacitor bank is indicated by a 20μA API (Assembly Products, Inc.) meter relay, connected in series with a 200 MΩ resistor and calibrated as a voltmeter. It also is the main controlling element in the charging system which interrupts the charging process at the preset voltage.

2. Charging Control System

A diagram of the charging control curcuit is given in Figure 15. In the "charging" condition relay R_1 is closed, switch 2 open. As soon as the preset voltage is reached and the pointers of the meter relay make contact, R_1 is energized and reverses the position of switches 1 and 2. Closing the "fire" push button activates R_2 and in turn de-energizes R_1. The system is back in the charging condition.

Indicator lights are connected as shown. As a safety precaution a charge warning flasher and a microswitch at the fume hood window have been included in the charging circuit. Opening of the sliding window has the same effect as putting S_2 into "dump" position: interruption of the charging process and dumping of any charge on the capacitor bank.

3. Trigger Circuit

The flashlamp trigger circuit (Figure 16) consists of a Dressen-Barnes 300 volt, 70 μA DC power supply, an 8μF oilfilled capacitor and an ILC Model T105 trigger transformer with a step-up ratio of 60:1. The circuit is controlled by a relay, R_2, that is energized by pressing the "fire" push button.

4. Gas Handling Control System

The remote control operation of the valves in the vacuum system was necessary due to the hazardous characteristic of some of the substances used as mentioned earlier. Not only was it necessary to open and close the valves from a remote control panel (as shown in Appendix G) but it was also desirable to have an indication of the state of each valve at a glance in order to avoid accidental operation of valves. The circuit designed to both control the solenoids for operation of the valves and drive the indicator lights is given in Figure 17. Only two of the solenoids are shown in the drawing. The others are omitted for simplicity. In addition, the connection of the reversible AC motor that opens and closes stopcock A in Figure 9 is shown.

Operation of the switches for valve control at the panel (S_3 and S_4 in Figure 17) energizes the solenoids that open the valves. At the same time an indicator light bulb lights up on the panel. The operation of the indicator

lights can be checked separately without energizing the solenoids by closing check switch S_4.

F. OPTICAL SYSTEM

The optical system consists of the light generator (laser tube), light amplifier (resonant optical cavity), and light detector. An alignment arrangement, although in itself not part of the optical system, is required to adjust the system components to the optical axis. A schematic is given in Figure 18.

The laser tube is 60 centimeters long with an inner diameter of 20 mm and wall thickness of 1.5 mm. It consists of fused quartz with 38 mm diameter, 4 mm thick, sodium chloride windows. One window, w_2, is attached at the Brewster angle of 56°40' (for sodium chloride) to minimize reflection, but the other, w_1, is attached at 40° to reflect on each pass approximately 1.5% of the incident radiation [Ref.15]. To avoid losses from mismatched polarization of the created light, the ends of the laser tube have to be cut carefully at the specified angle such that the smaller axes of the ellipses created by the cut are exactly parallel. To achieve this, the following method was used:

The ends of the laser tube were cut roughly at the desired angle. Then the tube was mounted on a bench as shown in Figure 19 with one of the ends resting on a turntable with some grinding compound. By moving the tube mount as indicated, any desired angle can be accurately obtained.

Moreover, after turning the tube by 180° around its transverse axis the other end will be ground as specified above. The finished laser tube is mounted on a standard laboratory type optical bench with its longitudinal axis parallel to the center line of the bench.

The optical cavity is formed by two stainless steel (coated with nickel-chromium) spherically concave mirrors of radius R_1 = 4 meters and R_2 = 10 meters. The mirrors are placed a distance L = 78 cm apart in gimbal mounts on the optical bench, one on each side of the laser tube and aligned with it. In this arrangement the stability conditions for confocal resonators with mirrors of unequal radii are fulfilled (Appendix D).

The spot sizes of the laser beam on the two mirrors can be calculated using Gaussian beam theory [Ref.25]. The following relations apply:

$$r_1^2 = \frac{L\lambda}{\pi}\left[\frac{g_2}{g_1(1-g_1g_2)}\right]^{1/2} \qquad (4\text{-}12)$$

$$r_2^2 = \frac{L\lambda}{\pi}\left[\frac{g_1}{g_2(1-g_1g_2)}\right]^{1/2} \qquad (4\text{-}13)$$

where r_1, r_2 are the radii of the spots on mirrors M_1 and M_2 and

$$\left.\begin{aligned} g_1 &= 1-\frac{L}{R_1} \\ g_2 &= 1-\frac{L}{R_2} \end{aligned}\right\} \qquad (4\text{-}14)$$

From these equations the spot radii are found to be, for $\lambda = 10.6\mu m$,

$$r_1 = 2.35 \cdot 10^{-3} \text{ (meters)}$$

$$r_2 = 2.20 \cdot 10^{-3} \text{ (meters)}.$$

The diameter of the larger spot is twice r_1 or 4.7 millimeters. This spot size applies to the lowest order mode. The comparatively large diameter of the laser tube, however, also allows higher order modes to exist which extend further in the transverse direction and have most of their energy off axis. The actual spot size may therefore be bigger than calculated above. Since in this experiment the modes of oscillation are of minor importance, no further discussion of this subject will be presented.

The amount of light decoupled from the cavity by window W_1 is reflected by a plane front coated mirror, M_4, from where it falls at right angles onto the light sensitive element of an infrared detector. The detector used is a gold doped germanium photoconductive infrared detector that requires cooling by liquid nitrogen. The sensitive element is mounted in a side-looking design dewar package with a liquid nitrogen holding time of approximately 6 hours. The device is sensitive to radiation from 1.0 to approximately 10 microns. At the expected CO_2 laser radiation of 10.6 μm the detector output is 1 volt for every watt of IR input with a response time of less than one microsecond. The bias

arrangement for the detector is shown in Figure 20. The output is fed directly into the preamplifiers of a Model 551 Tektronix oscilloscope.

For the alignment of the optical system a commercial He-Ne laser is used with a continuous output of one milliwatt of red light. An alignment procedure is given in Appendix E.

V. EXPERIMENTAL RESULTS

A. PRELIMINARY EXPERIMENTS

After the construction of the laser system was completed several experiments were carried out to test individual sections of the system.

1. Operation of the Charging and Triggering System

A number of modifications and improvements were found necessary before the final design as described in Section IV-E was arrived at. A listing of the changes made would contribute little to the understanding of the system operation and would be beyond the scope of this work. One modification, however, should be mentioned. After the original low power 500V supply of the triggering circuit was damaged by overheating it was replaced by the 300V supply presently used because a more powerful 500V supply was not immediately available. A series of flash experiments showed that even at discharge voltages as low as 4.5 KV the flashlamp could be reliably triggered.

2. Operation of the IR Detector and Photomultiplier

For the detection of the light output from the flashlamp a photomultiplier tube was originally used. The pulse duration obtained was approximately 1000μsec, as compared with the expected value of 100μsec. In control experiments using the infrared detector it was found that the long fall time of the PM was responsible for this (Figure 21);

the same experiments also showed that the rise time of the photomultiplier is of the order of 100μsec.

The output from the IR detector (Figure 27) indicated that its response sufficiently overlaps with the spectral range of the flashlamp output to make it useful for the detection of the light input to the laser. The rise time of the light pulse as measured by the IR detector was about 30μsec which agrees with the expected value. The fall time, however, was even longer when measured with the IR detector than it had been with the photomultiplier. This indicates that the infrared detector was saturated and its output possibly influenced by other effects in addition to the light flash.

To get a more correct shape of the light pulse the IR detector was removed from the immediate neighborhood of current carrying leads and the light input was decreased by using an aperture with a small pinhole in front of the detection crystal. In addition, the detector was directed toward the wall and shielded from the flashlamp by a metal sheet to avoid effects from heat radiation from the lamp. The pulse shape of the light flash obtained in this arrangement is shown in Figure 28. On the same photograph the shape of the current pulse in the discharge current lead is given. Figure 29 shows the detector output of the light flash with the detector in proper position for the detection of lasing action. An "Irtran" filter has been used to decrease the light intensity in the visible. The picture

clearly shows that the current pulse for the discharge current lead is picked up by the detector and superimposed on the detected light pulse. It is suggested that in further experimentation, the IR detector be relocated at a distance as far from any current leads as it is possible within the narrow dimensions of the fume hood and that a copper wire mesh be put around the detector to minimize pickup from any sources other than the light to be detected.

The total pulse duration of the light flash in Figure 28 is about 250μsec, still more than twice as long as expected. The current pulse in Figure 28, however, is only about 100μsec long which might indicate that the flash duration could be shorter than indicated by the detector.

3. Operation of the Discharge Circuit

The discharge circuit was designed to deliver a current pulse of critical damping, as shown in Figure 12. The actual pulse shape has been determined in several flash discharges at voltages between 5 and 8 KV to be an underdamped pulse with Figures 28 and 31 giving typical examples. The current has been measured by winding four turns of an insulated single wire lead around the high current lead and connecting the ends of the wire to the oscilloscope. The explanation for the underdamped pulse is very likely to be the arc inductance that, as pointed out in Section IV-D, becomes important at pulse durations below 100 to 150μsec. From Equation (4-6) it can be seen that the damping factor can be increased by decreasing the inductance. It is

suggested, therefore, that prior to further experimentation the inductance L in the discharge circuit be decreased by short circuiting part or all of the turns. Because the arc inductance can only be guessed by comparing the actual current pulse with Figure 12 - a short calculation using Equation (4-6) and assuming a damping factor of approximately 0.6 for the current pulse indicates an arc inductance roughly two times as big as L -, this should be done in steps and the change of the current pulse shape recorded in repeated discharges.

The capacitor voltage was measured using a Tektronix high voltage probe with a step-down ratio of 100 to 1. The voltage change during the discharge is shown in Figures 30 and 31. The shape of the curves also indicates a shorter pulse duration than was obtained from the IR detector, approximately 150μsec. Here the sharp voltage drop in the first part of the curve is assumed to be due to the flash discharge, whereas the following slow decrease is assumed to be caused by an afterglow of the lamp.

4. Operation of the Vacuum System

The remote control operation of the vacuum system has caused no problems. All major leaks have been found and sealed. Due to the many connections in the system - every valve alone requires two connections - smaller leaks have not all been found and a helium leak detector will have to be employed. However, since the system is not designed as a high-vacuum system, a small amount of leakage can not be

completely avoided. At the present time leakage amounts to a pressure increase of approximately 5 mm of mercury per hour.

VI. SUMMARY

The major objectives of this project were to design and construct a chemical CO_2-HN_3 laser system with initiation by photolysis of HN_3. These objectives have been achieved, a complete laser system has been developed and its major parts been tested. Possible improvements are suggested.

The major accomplishments in the development of this system are summarized as follows:

1. A quartz laser tube with NaCl Brewster windows was designed and fabricated.

2. A linear high power flashlamp was selected and installed.

3. Design and construction of a corrosion resistant remote control gas handling system.

4. A remote control HN_3 generating system was developed.

5. A high power flashlamp driving system was designed and fabricated.

6. Design and installation of a reliable charging and control system.

7. Arrangement of the vacuum and generating systems inside a fume hood with an exhaust to the outside.

In addition, the basic principles and equations governing the operation of a CO_2-N_2 laser system have been included.

APPENDIX A: VIBRATIONAL RELAXATION TIMES

The vibrational relaxation times are taken from the survey of Taylor and Bitterman [Ref.12] and from Ref.26. Included are relaxation due to collisions with CO_2, N_2, and He.

$$p\tau_a(CO_2\text{-}N_2) = 1.3\cdot10^5(T^{-1/3})^{4.9}$$

$$p\tau_a(CO_2\text{-}CO_2) = \left[\frac{0.73}{1700}(T\text{-}300) + 0.27\right] p\tau_a(CO_2\text{-}N_2)$$

for $T \leq 2000°K$

$$p\tau_a(CO_2\text{-He}) = p\tau_a(CO_2\text{-}N_2)$$

$$\log[p\tau_b(N_2\text{-}N_2)] = 93(T^{-1/3}) - 4.61$$

$$p\tau_b(N_2\text{-}CO_2) = p\tau_b(N_2\text{-}N_2)$$

$$\log[p\tau_b(N_2\text{-He})] = 60.7(T^{-1/3}) - 4.168$$

$$\log[p\tau_c(CO_2\text{-}CO_2)] = 17.8(T^{-1/3}) - 1.808$$

$$p\tau_c(CO_2\text{-}N_2) = 4p\tau_c(CO_2\text{-}CO_2)$$

$$\log[p\tau_c(CO_2\text{-He})] = 5.76(T^{-1/3}) - 1.297$$

In the above correlations, $p\tau$ is in (μsec-atm.) and T is in (°K). At an assumed temperature of T = 300°K the relaxation times become:

$p\tau_a(CO_2\text{-}N_2)$ = 12.0 μsec-atm

$p\tau_a(CO_2\text{-}CO_2)$ = 3.24 μsec-atm

$p\tau_a(CO_2\text{-}He)$ = 12.0 μsec-atm

$p\tau_b(N_2\text{-}N_2)$ = $2 \cdot 10^9$ μsec-atm

$p\tau_b(N_2\text{-}CO_2)$ = $2 \cdot 10^9$ μsec-atm

$p\tau_b(N_2\text{-}He)$ = $80 \cdot 10^3$ μsec-atm

$p\tau_c(CO_2\text{-}CO_2)$ = 7.0 μsec-atm

$p\tau_c(CO_2\text{-}N_2)$ = 28.0 μsec-atm

$p\tau_c(CO_2\text{-}He)$ = 0.428 μsec-atm

APPENDIX B: OPERATION OF THE GAS HANDLING SYSTEM

A step-by-step procedure is given for the operation of the gas handling system. At the end of each step the open valves are listed to provide an additional control.

Preparation of Experiment

Capacitor bank not charged. Fume hood open.

1. Clean system, close all valves. [No valves open.]

2. Weigh desired amount of NaH_3, add mineral oil, shake. Remove stopcock from generating flask, pour mixture into flask, replace stopcock. [No valves open.]

3. Fill H_3PO_4 (syrupy) into storage container. [No valves open.]

4. Open S and T, flush with N_2 by opening and closing B. Close S. [Open: T.]

5. Open O, M, and I, flush with N_2 by opening and closing B. Close O. [Open: T, I, M.]

6. Open M2 and S. Switch on pump. Open P. Pump down. [Open T, I, M, M2, S, P.]

7. Close M2. Open M1 and fill pipette to the desired height. Close M1. [Open: T, I, M, S, P.]

Performing of Experiment

Capacitor bank charged. Fume hood closed.

8. Close T, S, and P. Drain H_3PO_4 by opening and closing A (motor takes 15 sec. to turn valve). Generate

HN_3. Fill x mm HN_3 into laser tube by opening and closing S. [Open: I, M.]

9. Open T. Add y_1 mm CO_2 by opening and closing C. [Open: T, I, M.]

10. Add y_2 mm N_2 by opening and closing N. [Open: T, I, M.]

11. Add y_3 mm He by opening and closing H. [Open: T, I, M.]

12. Close T, I, and M. Fire flashlamp. [No valves open.]

13. Flush system by carrying out steps 4 and 5. [Open: T, I, M.]

14. Remove and clean generating system. Replace, open M2, S, and P. Keep system evacuated until experiment is repeated. [Open: T, I, M, P, M2, S.]

The operation of the laser has not been part of this work. This will be accomplished by Francis G. Helmsin, also of the U.S. Naval Postgraduate School, who will continue with the project.

APPENDIX C: FLASHLAMP DRIVING CIRCUIT PARAMETERS

Data for the Flashlamp as Given by the Manufacturer:

Lamp impedance parameter:

$$K_0 = 80(\Omega\text{-amp}^{1/2})$$

Single shot explosion energy constant:

$$K_e = 1.3 \cdot 10^6(\text{joules-sec}^{-1/2})$$

Max average power (convection cooling):

$$P_{max} = 960(\text{watts})$$

Min required voltage:

$$V_{min} = 2700(\text{volts})$$

Operating Parameters:

Total Capacitance: $C = 31.4$ (μF)

Total Inductance: $L = 30.0$ (μH)

Total Resistance: $R = 0.0018$ (Ω)

Using data given in Refs. 24 and 27 the following calculations can be made:

Time Constant: $\tau = (LC)^{1/2}$

$$\tau = (30 \cdot 10^{-6} \cdot 31.4 \cdot 10^{-6})^{1/2}$$

$$\tau = 30.7(\mu\text{sec})$$

Pulse Duration (10% current points):

$$T = 3\tau$$

$$T = 92.1(\mu sec)$$

Explosion Energy:

$$E_x = K_e \tau^{1/2}$$

$$E_x = 1.3 \cdot 10^6 (joules \cdot sec^{-1/2})(30.7)^{1/2}(\mu sec)^{1/2}$$

$$E_x = 7.2 \cdot 10^3 (joules)$$

The explosion energy is the energy where the lifetime of the lamp is equal to one flash. For energies less than the explosion energy the lifetime is determined by the loading factor, λ, and the energy dissipated in one flash, E. The relationship can be approximated using Ref.27:

$$\text{Life (in flashes)} = \lambda^{-8.5} \qquad \text{(A-1)}$$

where

$$\lambda = \frac{E}{E_x} \qquad \text{(A-2)}$$

A graph of average lifetime vs. flash energy is given in Figure 21.

The flash energy E is a function of capacitor voltage V given by

$$E = 0.5C(V - V_4)^2 \qquad \text{(A-3)}$$

where V_r is the residual voltage that remains on the capacitor bank after the light flash extinguishes. This value has been found from preliminary experiments to be about 2000 volts. The values that V can take on are restricted by the requirement for critical damping. The damping factor, α, is given by Ref.27:

$$\alpha = \frac{K_0}{(VZ_0)^{1/2}} \qquad \text{(A-4)}$$

where

$$Z_0 = \left(\frac{L}{C}\right)^{1/2} = \left(\frac{30 \cdot 10^{-6}}{31.4 \cdot 10^{-6}}\right)^{1/2}$$

$$Z_0 = 0.975(\Omega)$$

From Ref.24, for critical damping the damping factor α_0 is

$$\alpha_0 = 0.8$$

The corresponding capacitor voltage, V_0, can be calculated from Equation (A-4) to be

$$V_0 = \frac{K_0^2}{\alpha_0^2 Z_0} = \frac{(80)^2(\Omega^2\text{-amp})}{(0.8)^2 \cdot 0.975(\Omega)}$$

$$V_0 = 10.25 \text{ KV}$$

To meet the warrantees regarding lamp life given by the manufacturer the capacitor voltage can be varied only such that

$$0.7 \leq \alpha \leq 1.1$$

The respective voltages are, from Equation (A-4):

$$5.43 \leq V \leq 13.4 \text{ KV}$$

The flash energies corresponding to these voltages are, from Equation (A-3) and assuming a V_r of 2000 volts:

$$185 \leq E \leq 2040 \text{ (joules)}$$

A graph of flash energy vs. capacitor voltage is given in Figure 22.

APPENDIX D: STABILITY REQUIREMENTS FOR CONFOCAL RESONATOR

A confocal resonator is stable, if [Ref.25]:

$$0 \leq g_1 g_2 \leq 1 \tag{A-5}$$

where

$$\left.\begin{aligned} g_1 &= 1 - \frac{L}{R_1} \\ \text{and} \\ g_2 &= 1 - \frac{L}{R_2} \end{aligned}\right\} \tag{A-6}$$

Here L is the length of the cavity and R_1, R_2 are the radii of the mirrors. Using Equation (A-6), the left hand inequality of Equation (A-5) can be written

$$0 \leq \left(1 - \frac{L}{R_1}\right)\left(1 - \frac{L}{R_2}\right) \tag{A-7}$$

This inequality has two solutions,

$$0 \leq \left(1 - \frac{L}{R_1}\right) \text{and } 0 \leq \left(1 - \frac{L}{R_2}\right) \tag{A-8}$$

or

$$0 \geq \left(1 - \frac{L}{R_1}\right) \text{and } 0 \geq \left(1 - \frac{L}{R_2}\right) \tag{A-9}$$

From Equations (A-8) and (A-9) it follows that

$$\left.\begin{aligned} L &\leq R_1, R_2 \\ \text{or} \\ L &\geq R_1, R_2 \end{aligned}\right\} \tag{A-10}$$

This means that the length L of the cavity must be either less than the smaller radius or more than the bigger radius.

For the right hand inequality of Equation (A-5) it is required that

$$\left(1 - \frac{L}{R_1}\right)\left(1 - \frac{L}{R_2}\right) \leq 1 \qquad \text{(A-11)}$$

or, after a little algebra,

$$L \leq R_1 + R_2 \qquad \text{(A-12)}$$

For the resonator to be stable, both Equations (A-10) and (A-12) must be true. For the values of L, R_1, and R_2 in the resonator under consideration ($L = 0.78$ meters, $R_1 = 4$ meters, $R_2 = 10$ meters), the inequalities (A-10) and (A-12) become:

$$0.78 \leq 4$$

$$0.78 \leq 4 + 10$$

which shows that the resonator is stable.

APPENDIX E: ALIGNMENT PROCEDURE FOR THE OPTICAL SYSTEM

The optical system is aligned with respect to the optical axis which is defined to be the line that passes through the center of the laser tube. The alignment laser is positioned at a distance of approximately 5 meters from the system in such a manner that its light beam intersects the optical axis of the system at the center of mirror M_3 (Figure 18). The alignment procedure is as follows:

1. Remove M_1, adjust M_3 until the light beam coincides with the optical axis (center of laser tube). M_3 remains in this position and needs no readjustment as long as the alignment laser is not moved.

2. Place the gimbal mount with mirror M_2 in position such that the light beam falls exactly onto the center of M_2. This can be achieved easily by temporarily replacing M_2 by a metal aperture with a small hole in the middle.

3. Align M_2 by turning the controls of the gimbal mount until the reflected beam coincides with the original beam.

4. Repeat steps 2 and 3 for M_1. Here the back side of the mirror (plane, stainless steel coated) is used for alignment, assuming that the mirror plane is perpendicular to the optical axis.

APPENDIX F: DRAWINGS

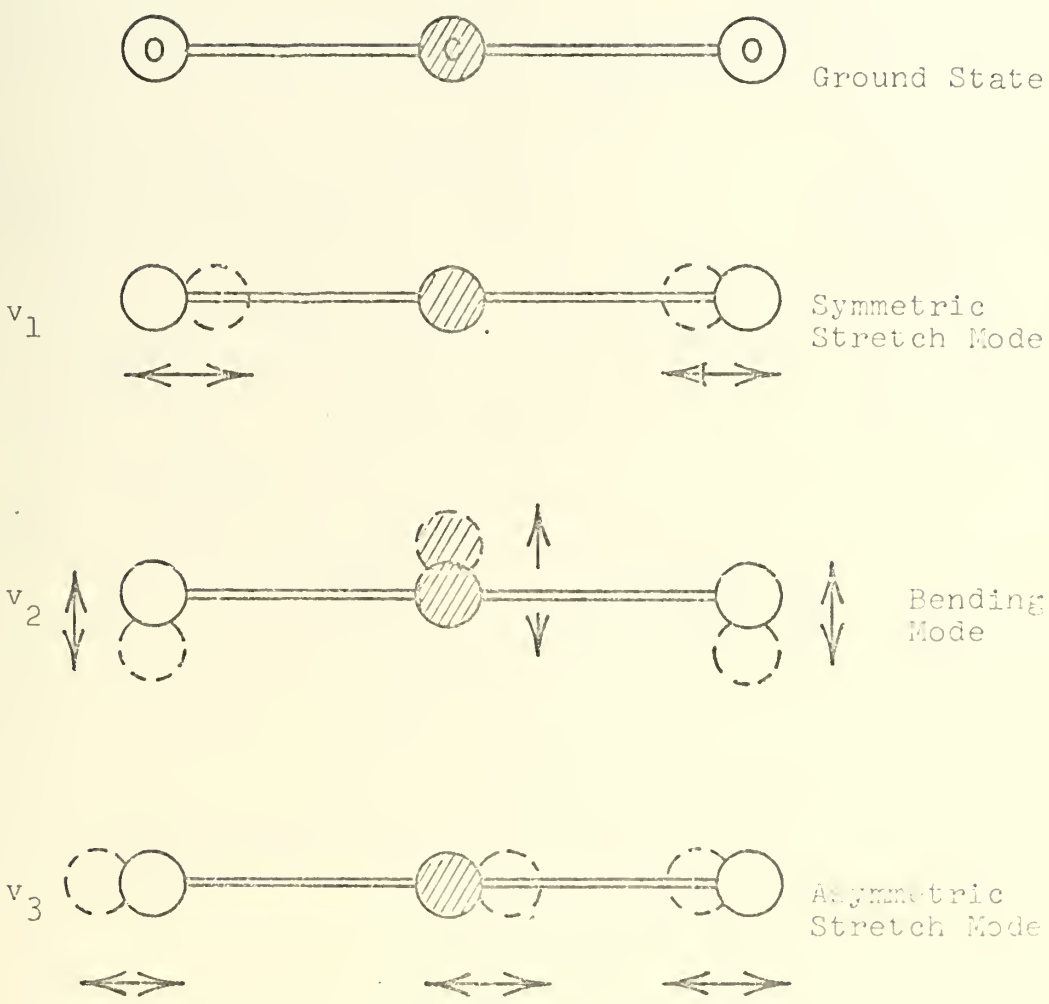

Figure 1. Vibrational States in the CO_2 Molecule

In the bending mode the atoms may vibrate in two mutually perpendicular planes, causing a twofold degeneracy with slightly different energy levels.

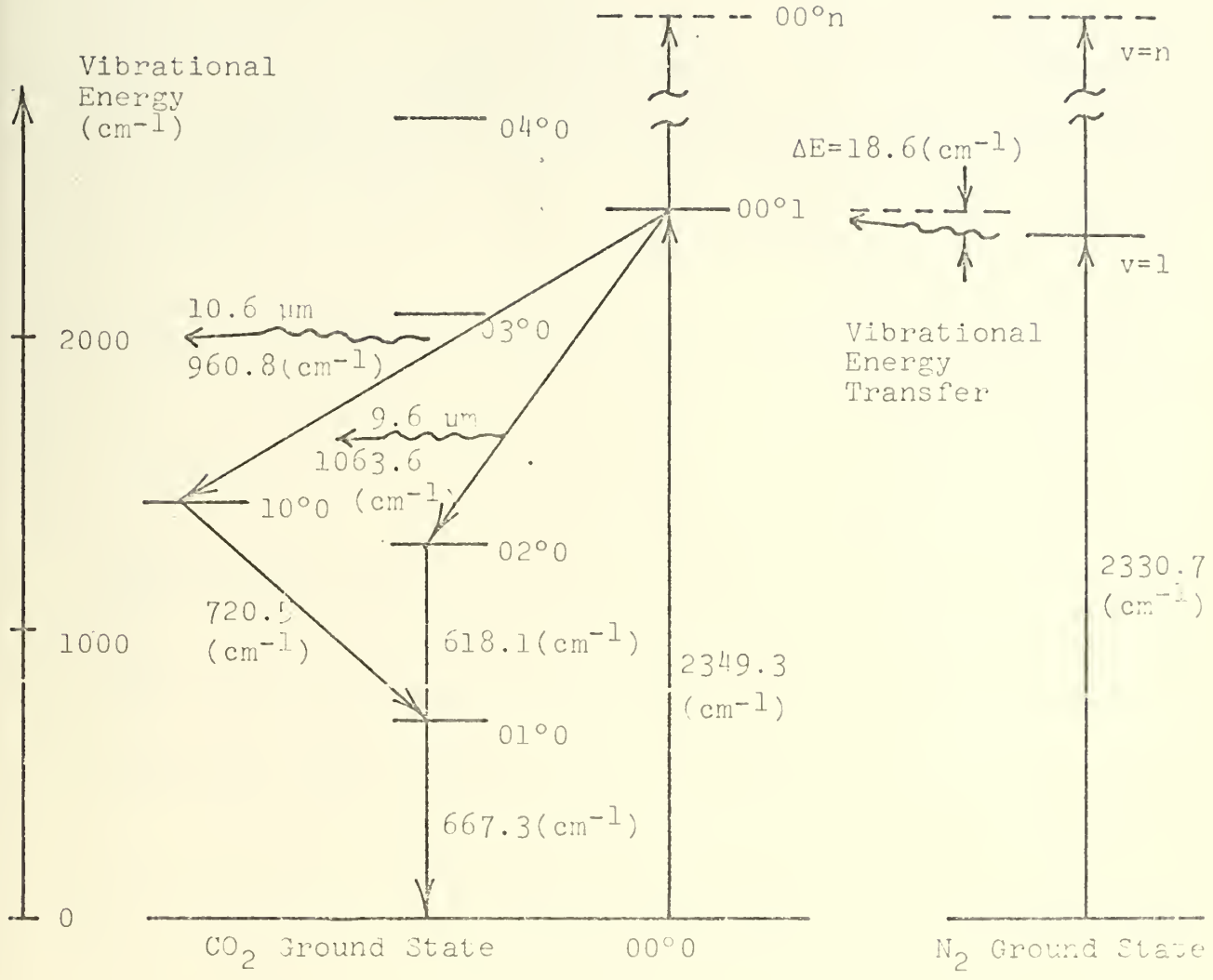

Figure 2. Pertinent Vibrational Energy Levels of CO_2 and N_2

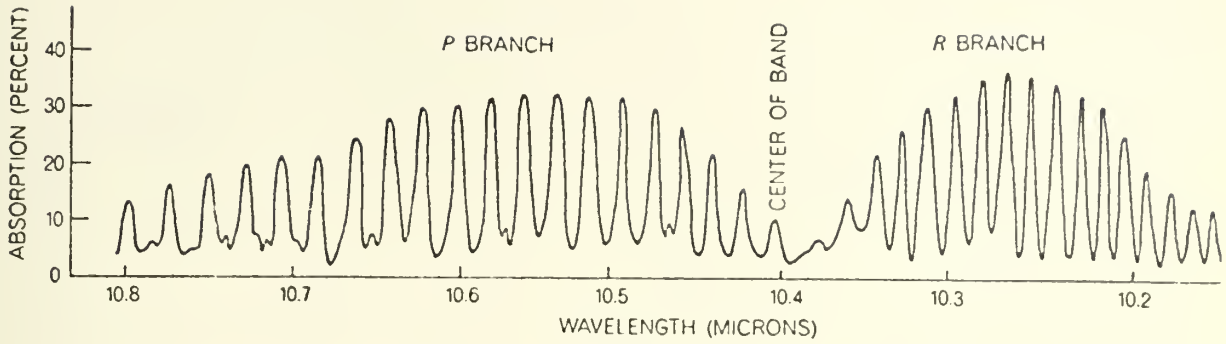

Figure 3. Rotational Transitions of the (00°1) → (10°0) Band in CO_2

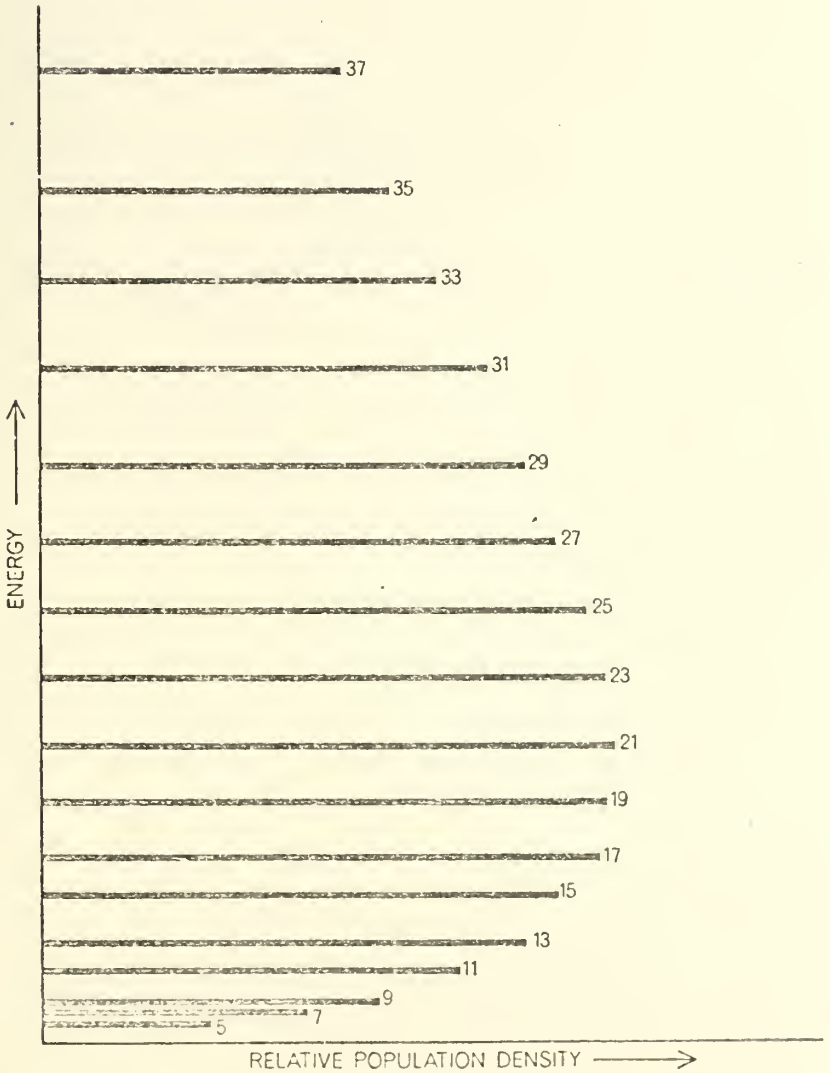

Figure 4. Rotational Energy Levels of the (001) Vibrational State of CO_2

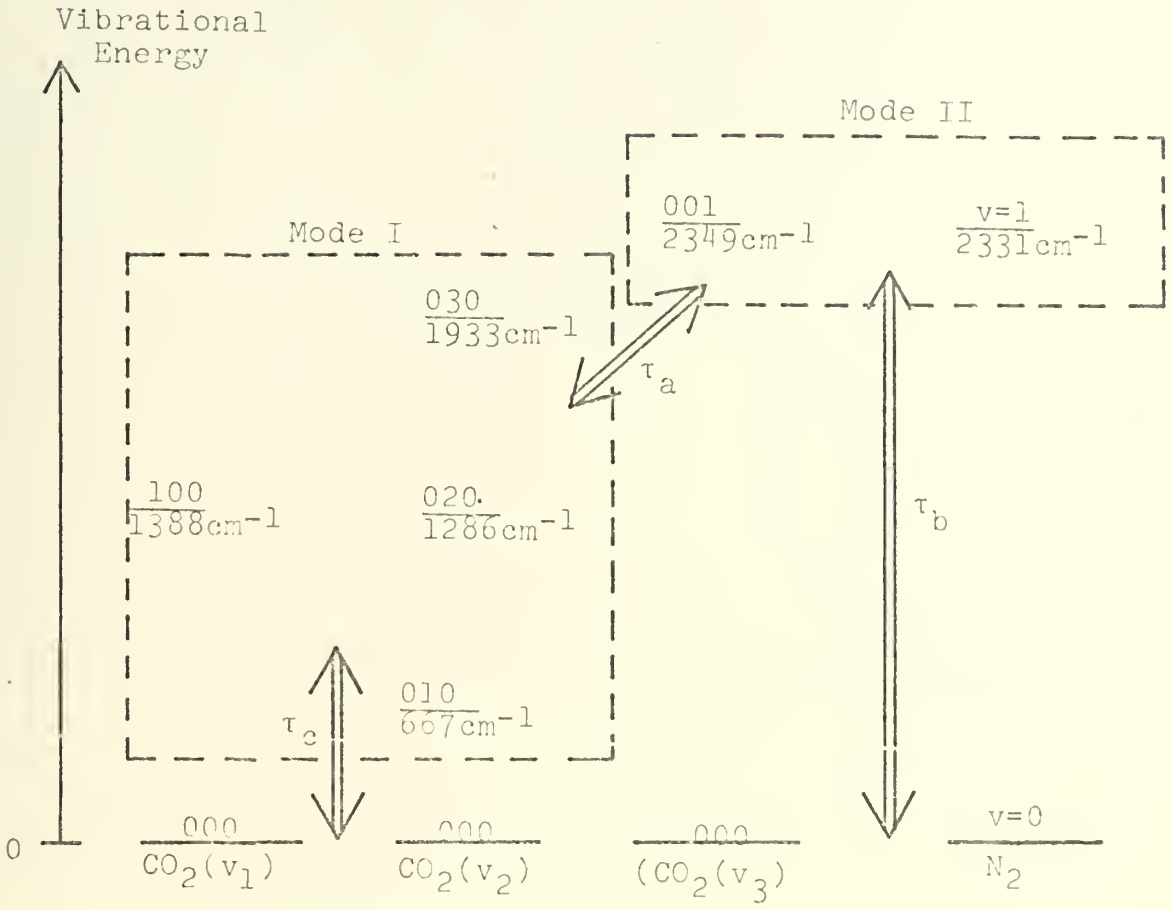

Figure 5. Vibrational Energy Levels for the Singlet

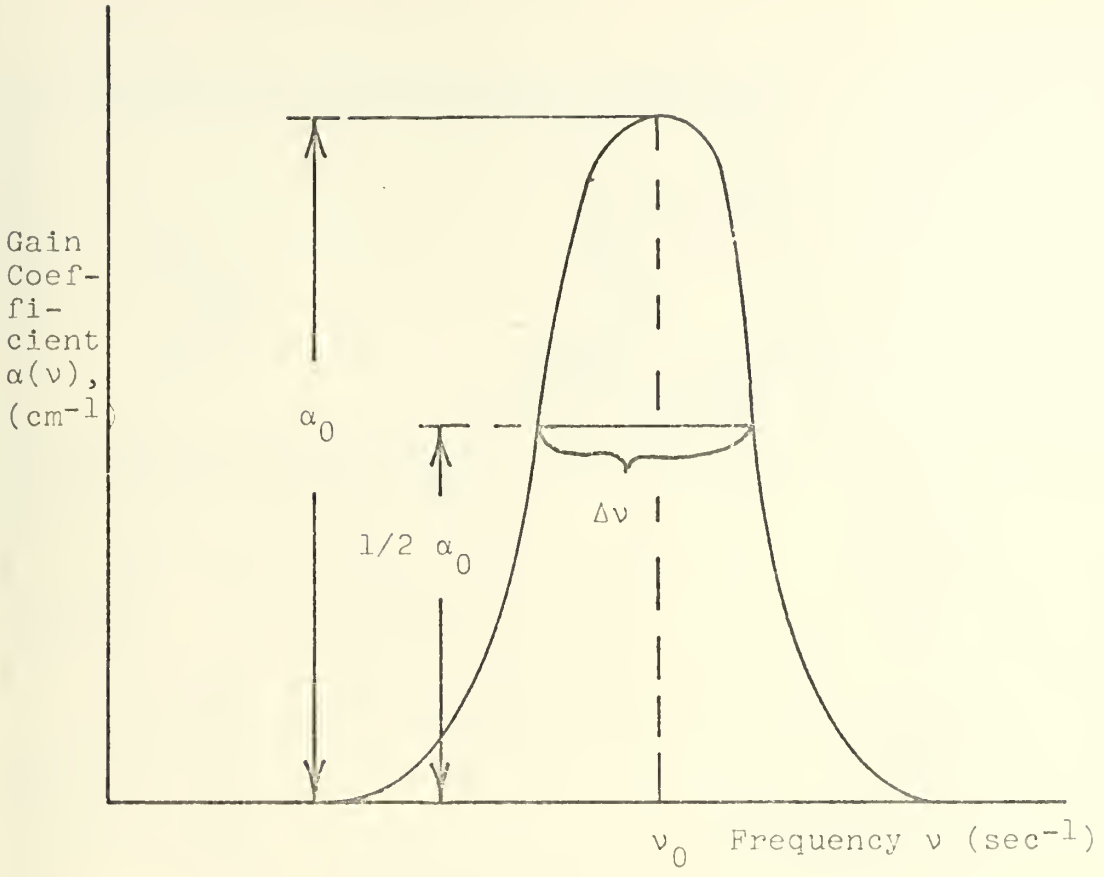

Figure 6. Gain Coefficient as Function of Frequency

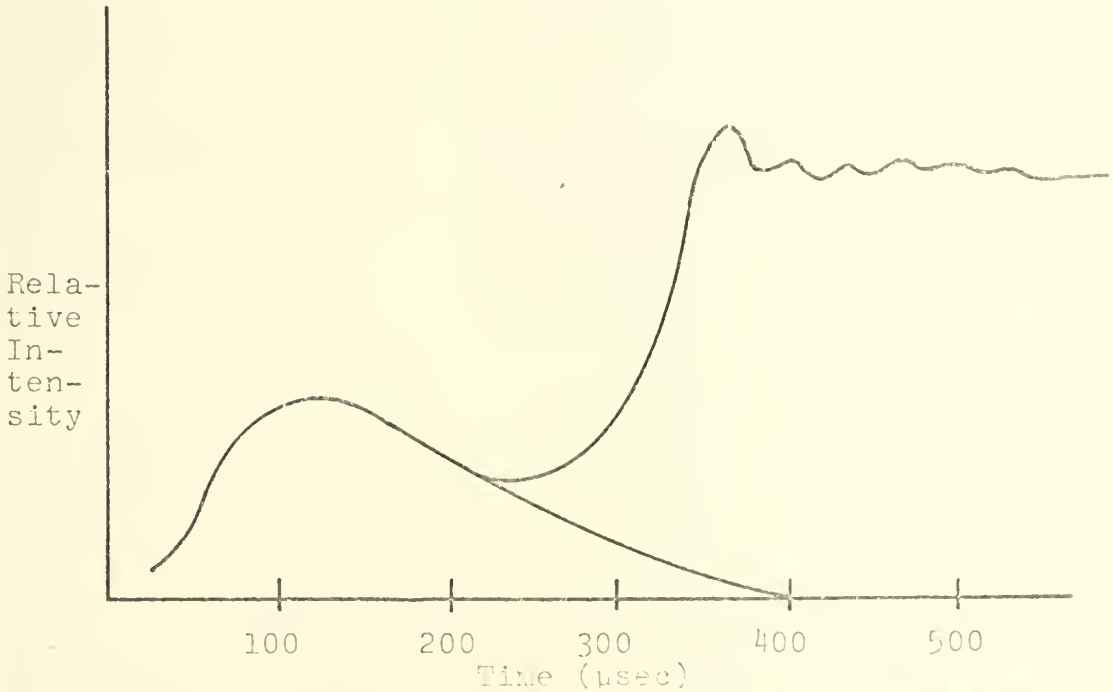

Figure 7. Flash Input and Lasing Output Intensities in CO_2-HN_3 Laser

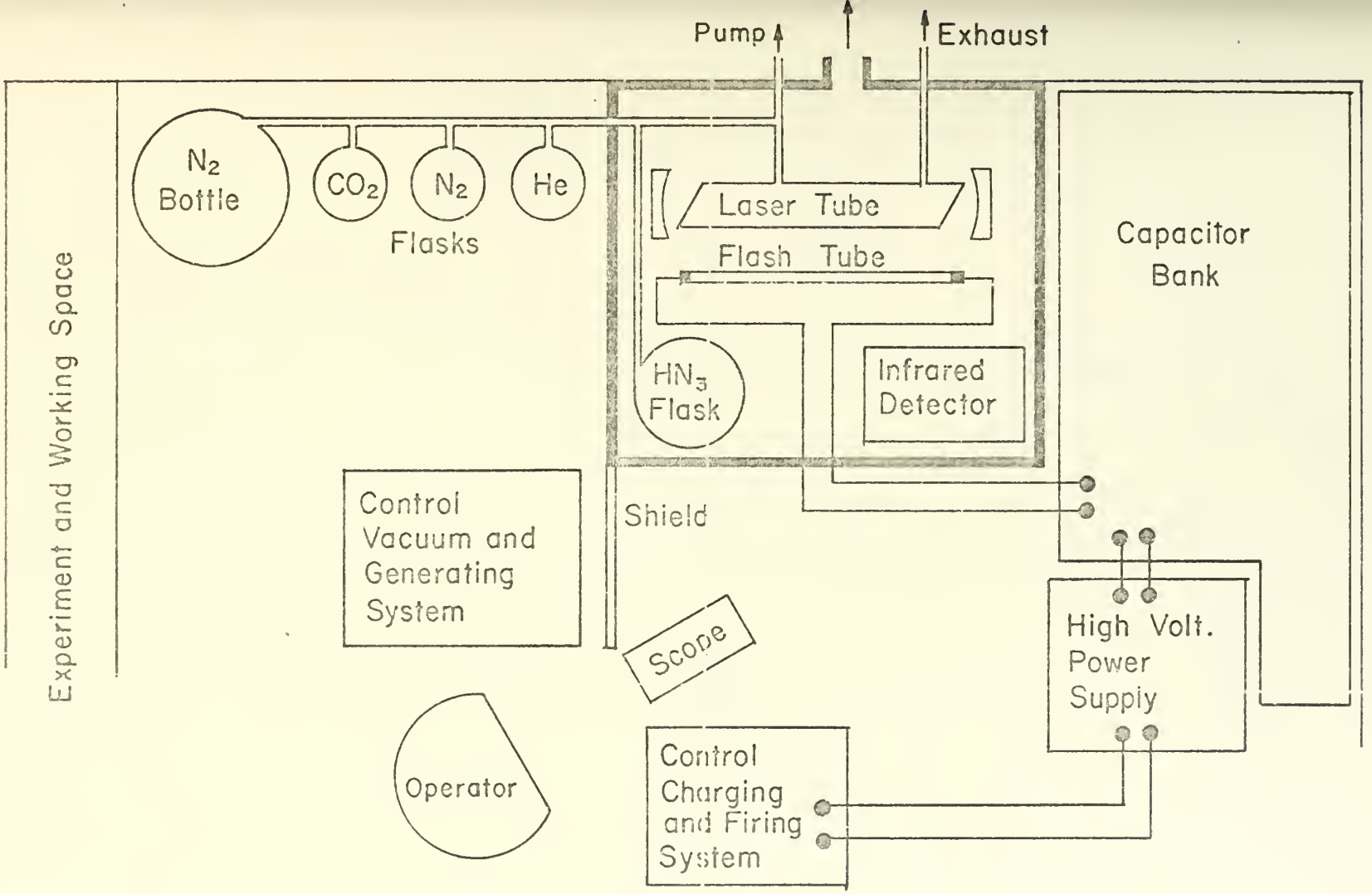

FIGURE 8. EXPERIMENTAL SETUP

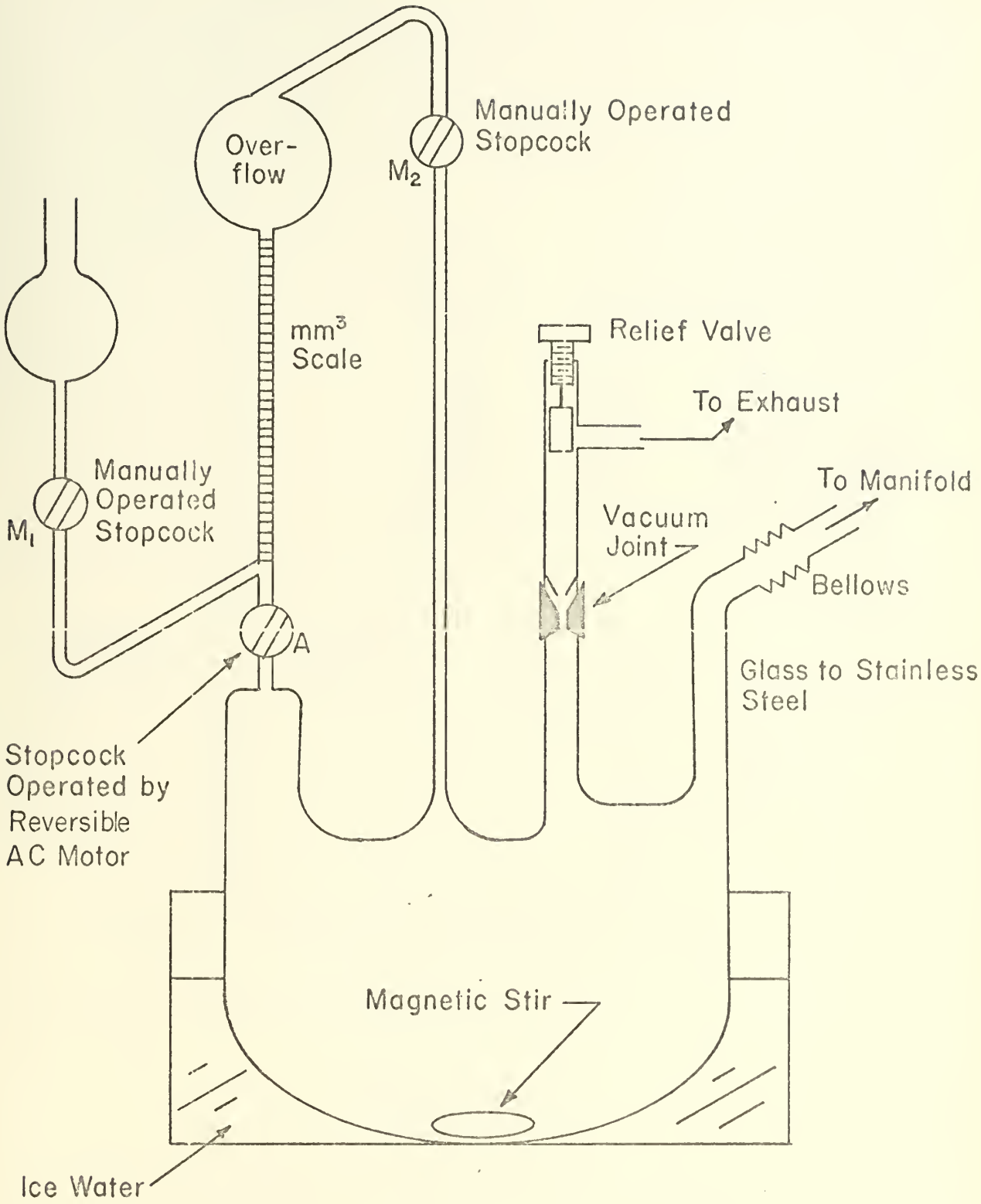

FIGURE 9. HN_3 GENERATING SYSTEM

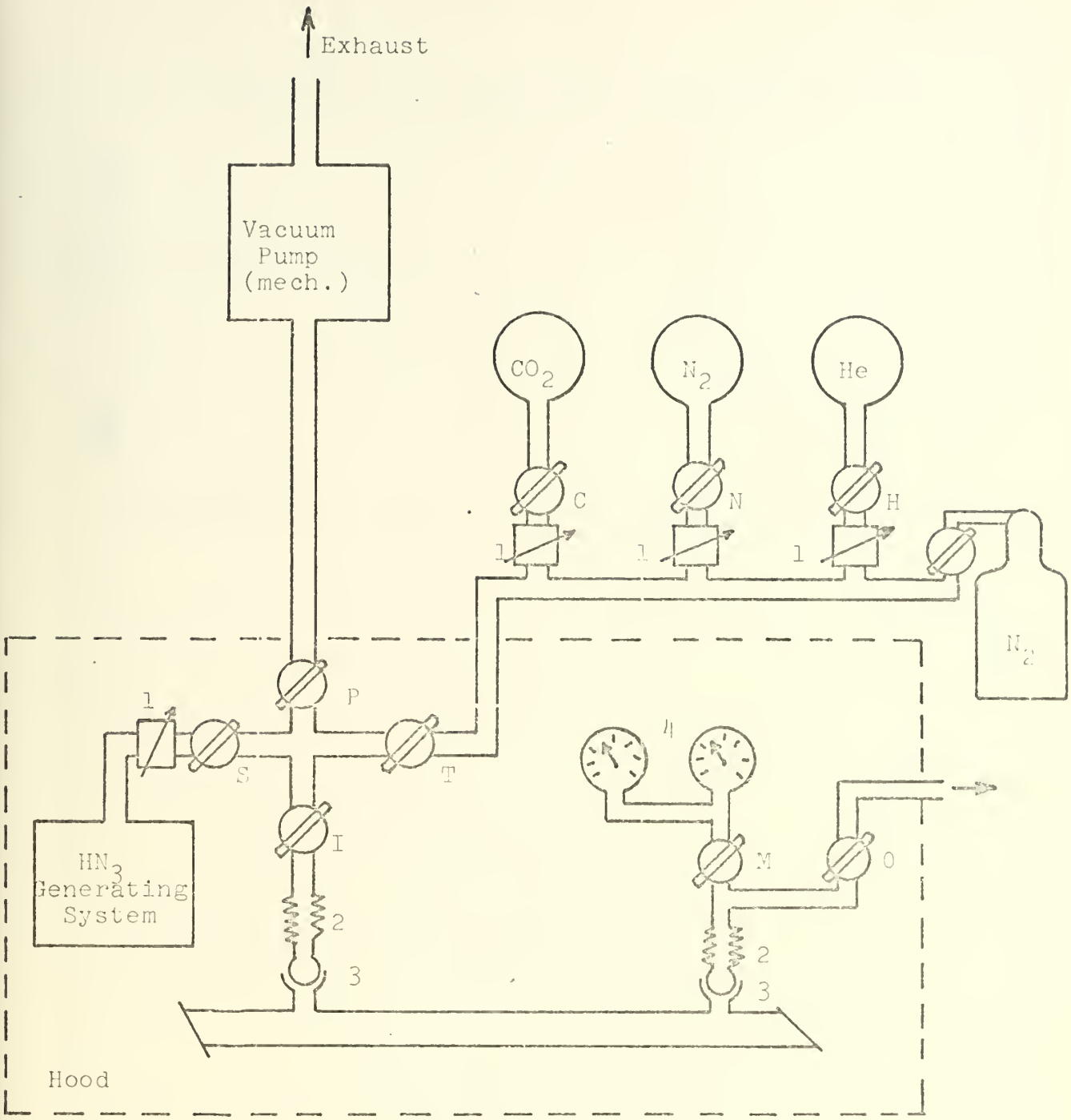

1. Needle valve and bypass
2. Stainless steel bellows
3. Balljoints
4. Bourdon tube and thermocouple gauge

Figure 10. Vacuum System

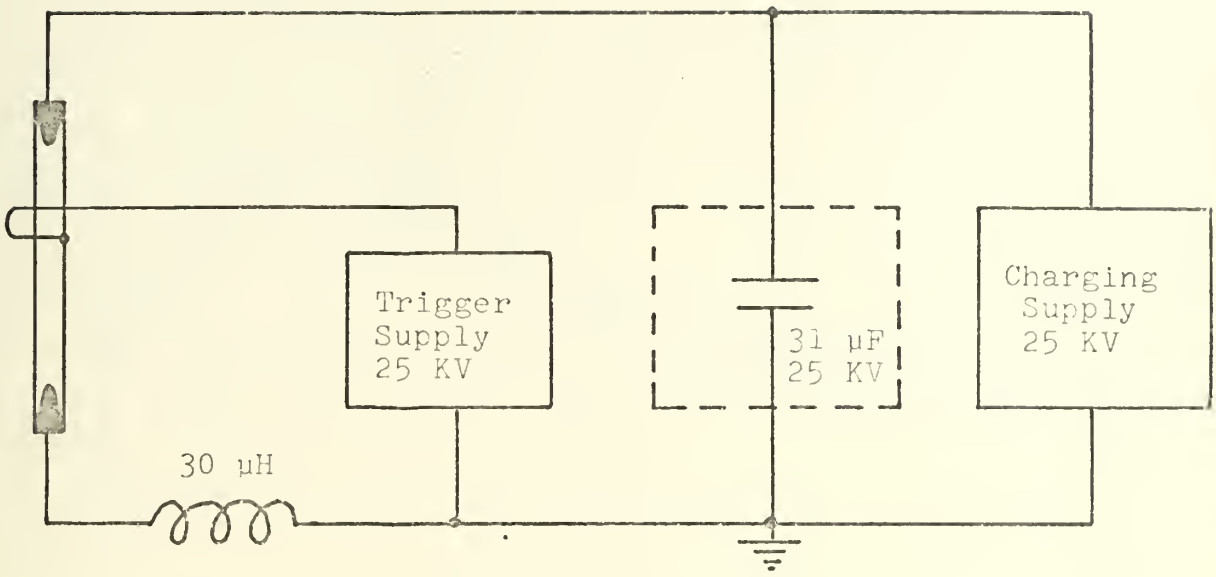

Figure 11. Flashlamp Discharge Circuit

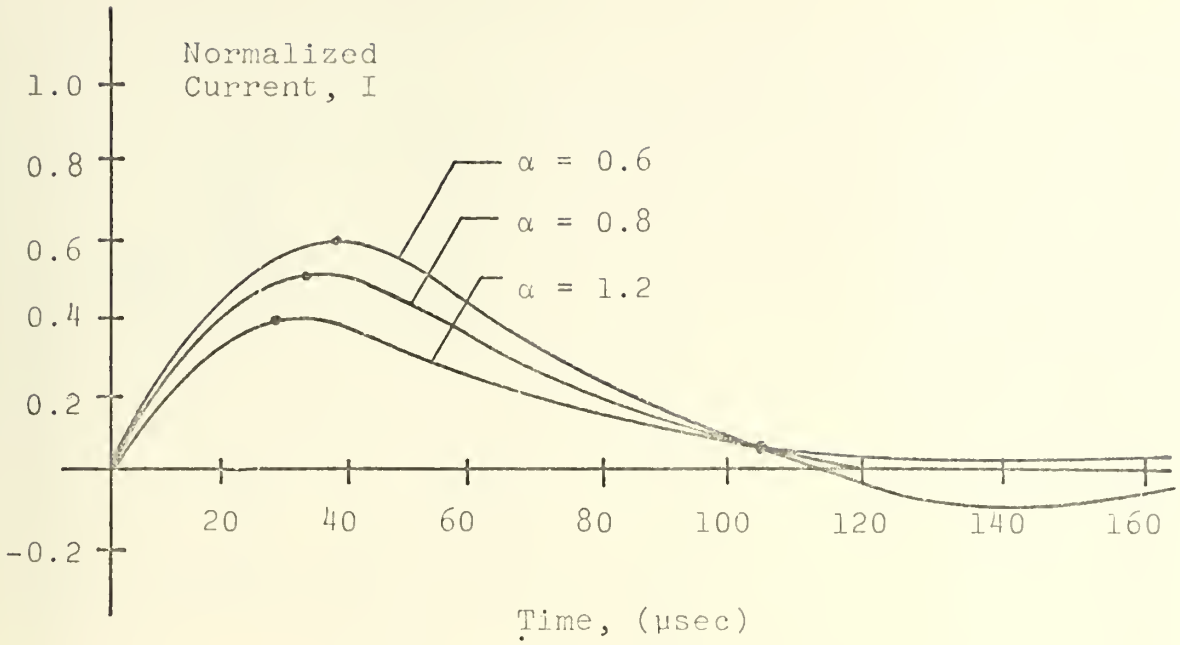

Figure 12. Normalized Flashlamp Current

α = 0.6 : underdamped

α = 0.8 : critically damped

α = 1.2 : overdamped

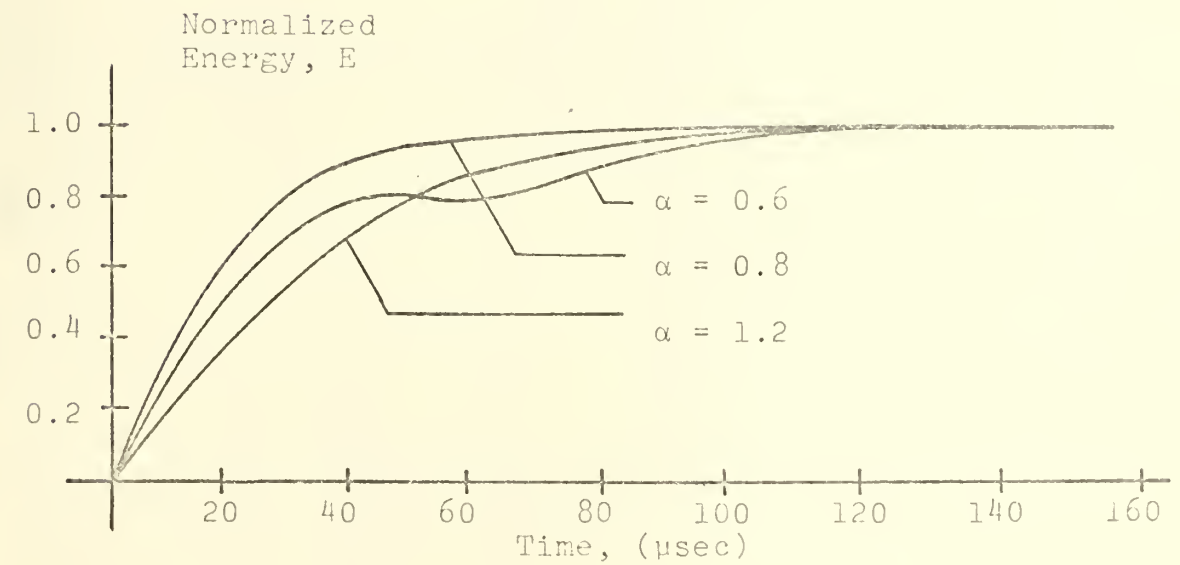

Figure 13. Normalized Flashlamp Energy

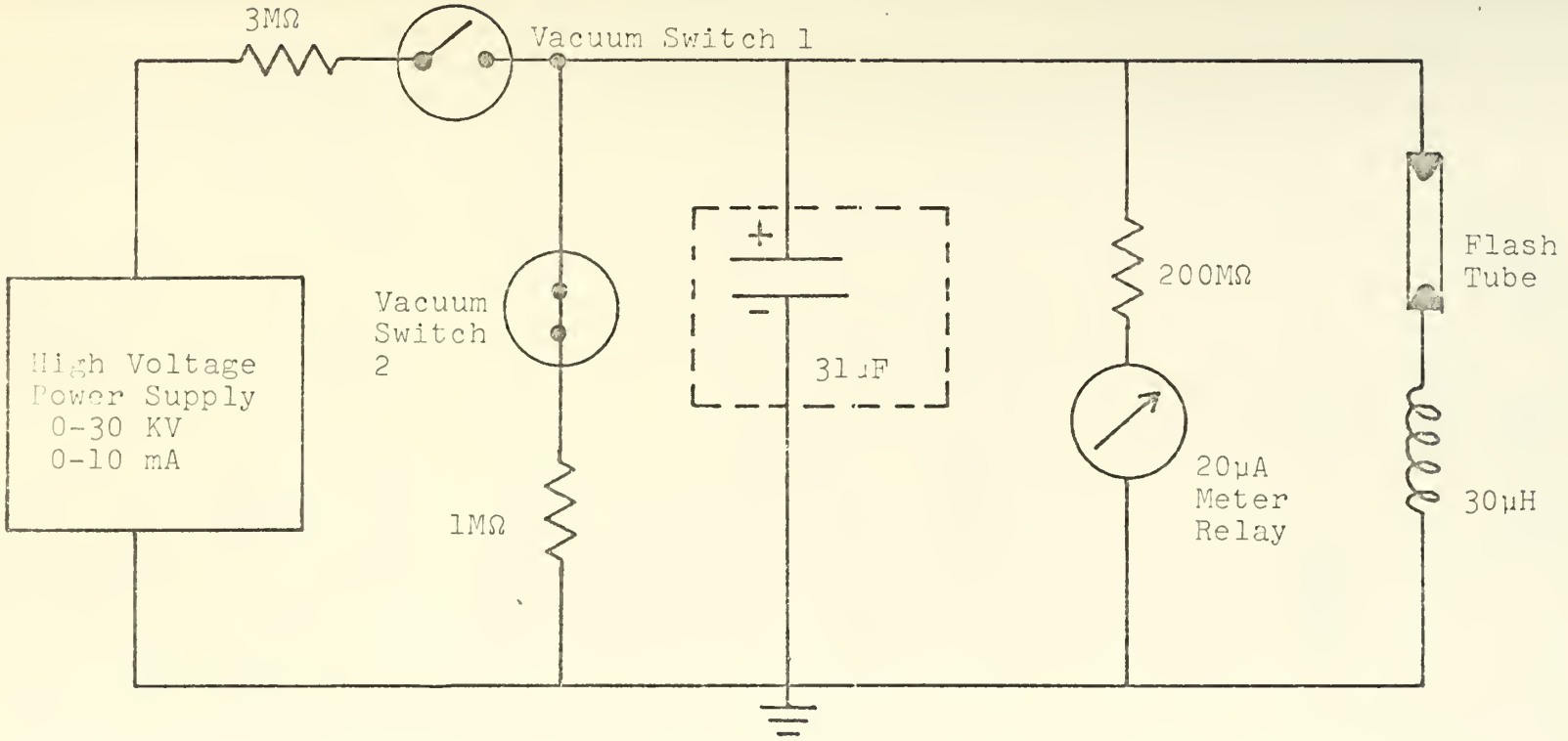

Figure 14. Block Diagram of Charging System.
Vacuum switches 1 and 2 are shown in normal (de-energized) position.

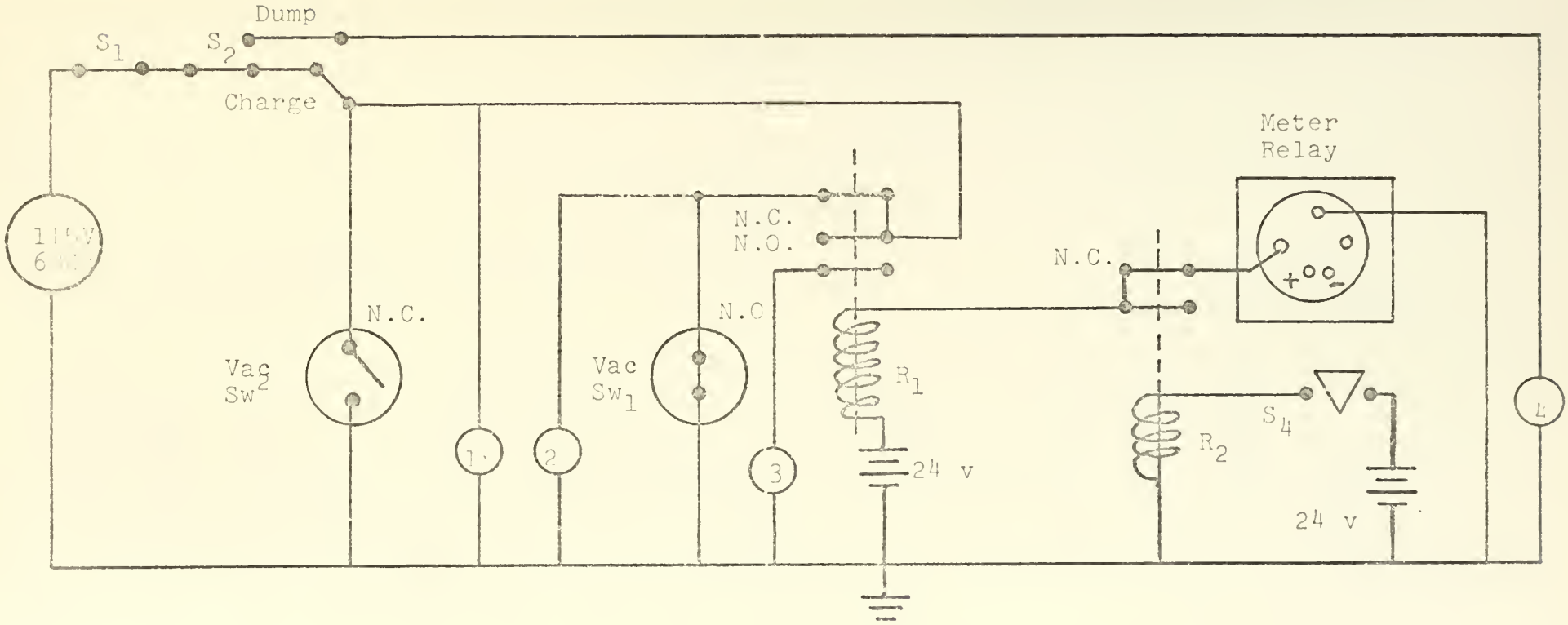

S_1: On-Off switch
S_2: Door safety interlock
S_3: Charge-Dump switch
S_4: "Fire" push button
R_1, R_2: 24 v DC Relay

1: Charge warning flasher
2: "Charging" indicator light
3: "Ready" indicator light
4: "Dumped" indicator light
N.O.: Normally open
N.C.: Normally closed

Figure 15. Charging Control System

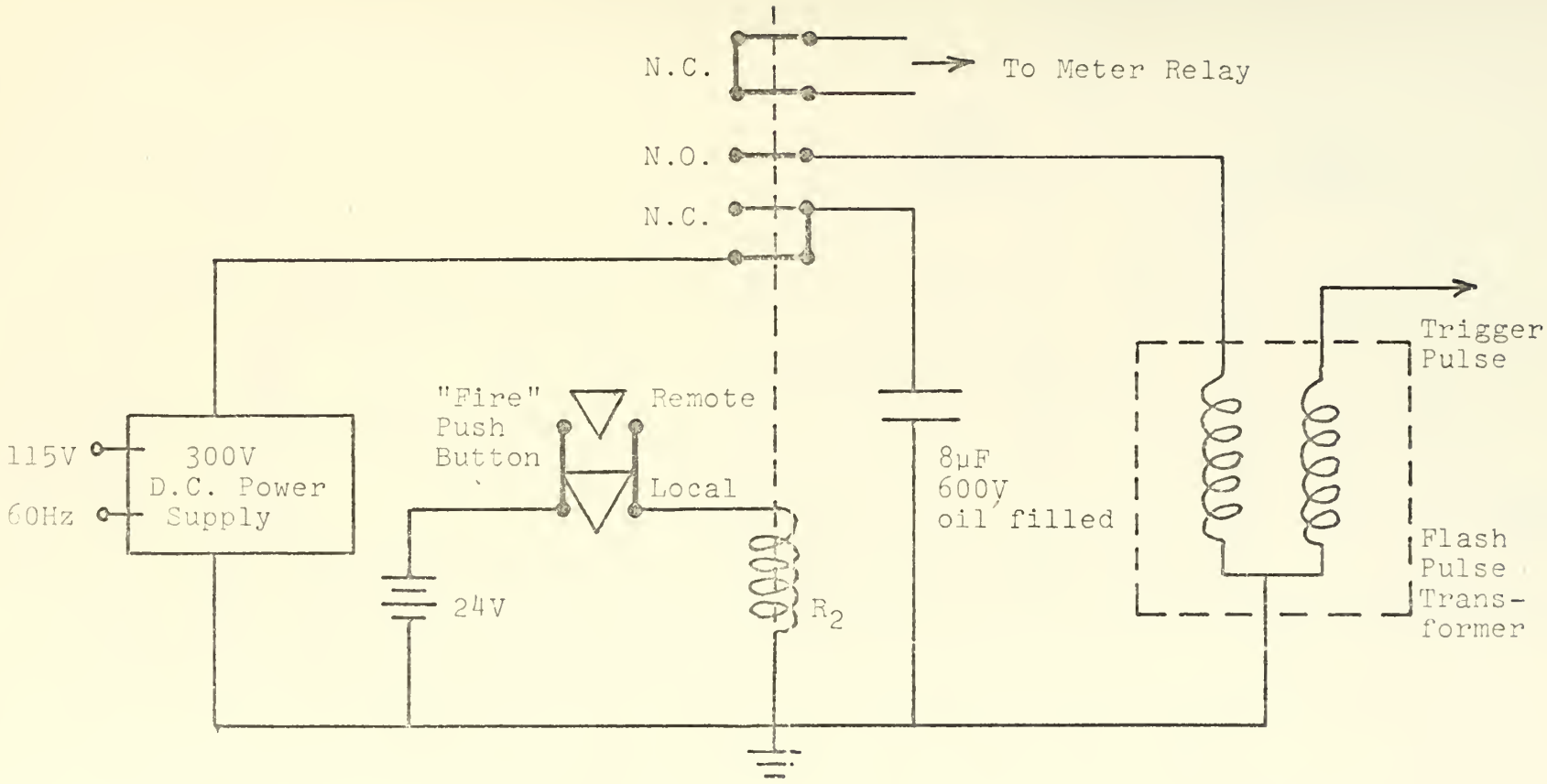

R_2: 24 V DC Relay

N.O.: Normally open

N.C.: Normally closed

Figure 16. Flash Lamp Trigger Circuit

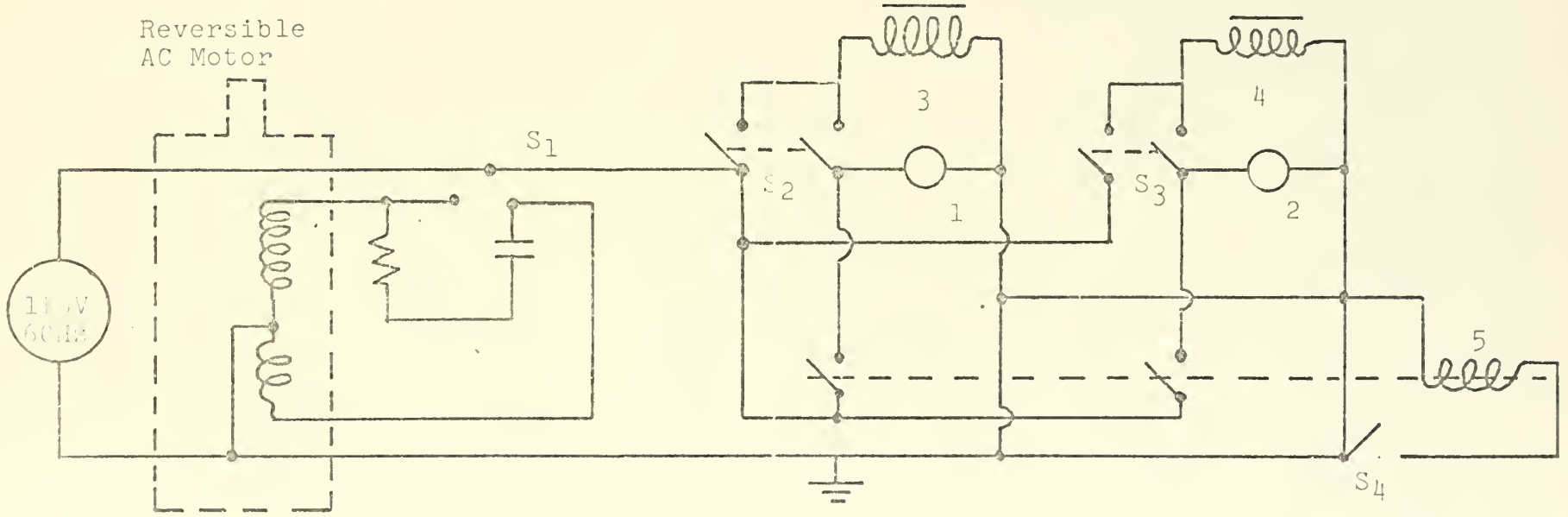

S_1: Stopcock control switch

S_2,S_3: Valve control switch

S_4: Indicator check switch

1,2: Indicator lights

3,4: Valve controlling solenoids

5: Light check solenoid

Figure 17. Circuit Diagram for Gas Handling Control System

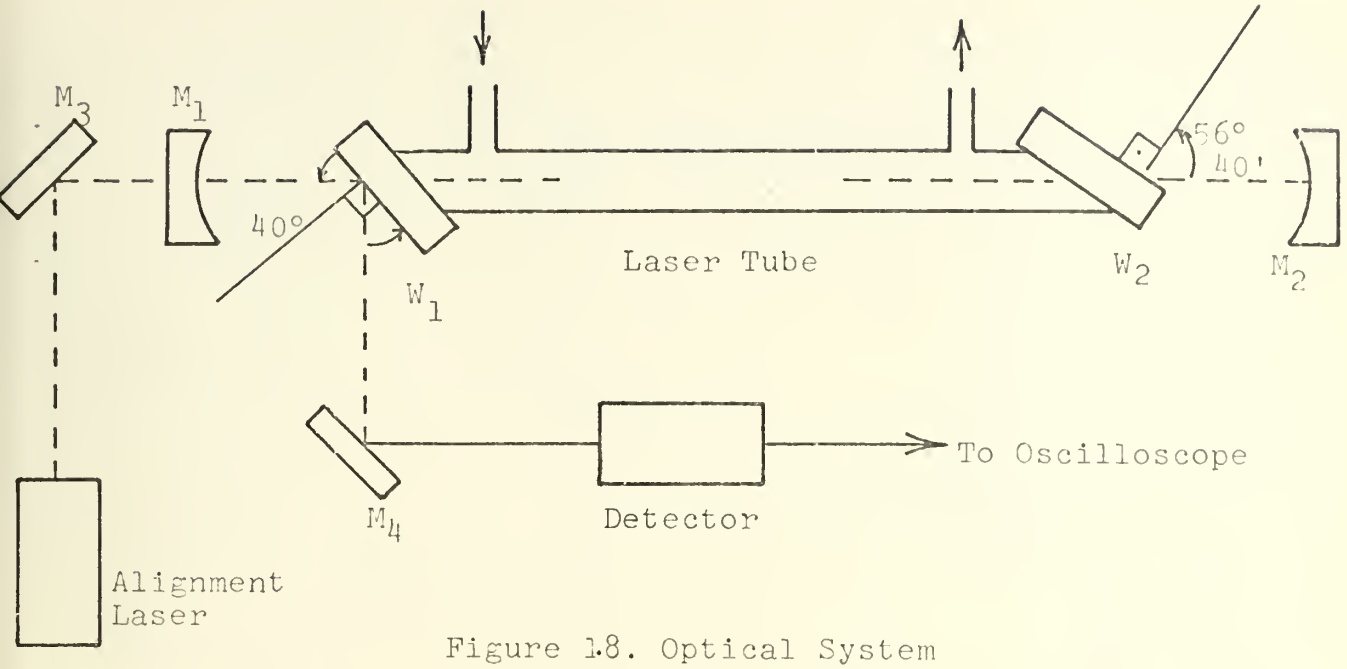

Figure 18. Optical System

M_1,M_2: Concave mirrors, 4 and 10 meters radius
M_3,M_4: Plane front coated mirrors
W_1,W_2: NaCl laser windows

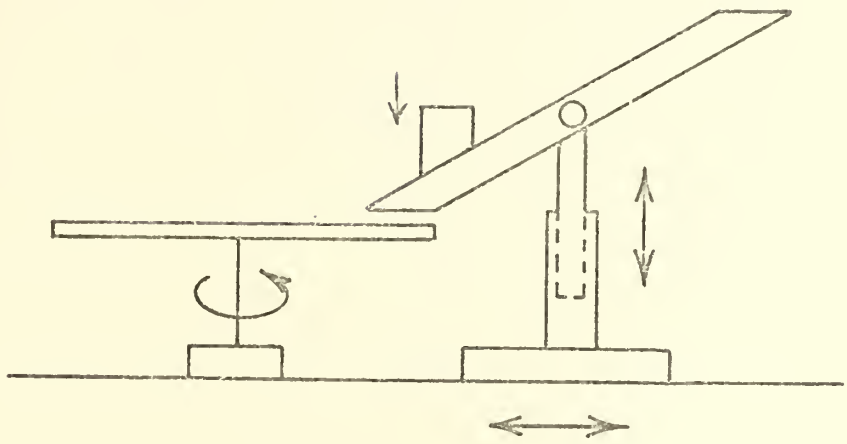

Figure 19. Schematic of Setup for Grinding of Correct Angles on Laser Tube Ends

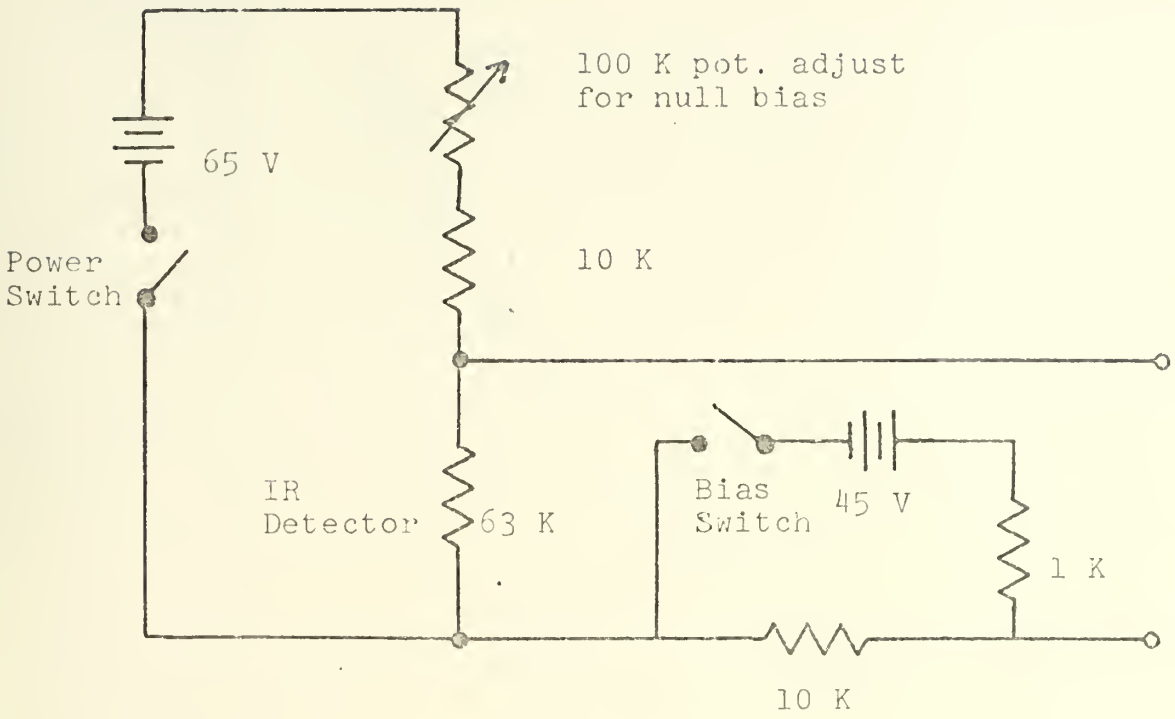

Figure 20. Biasing Circuit for IR Detector

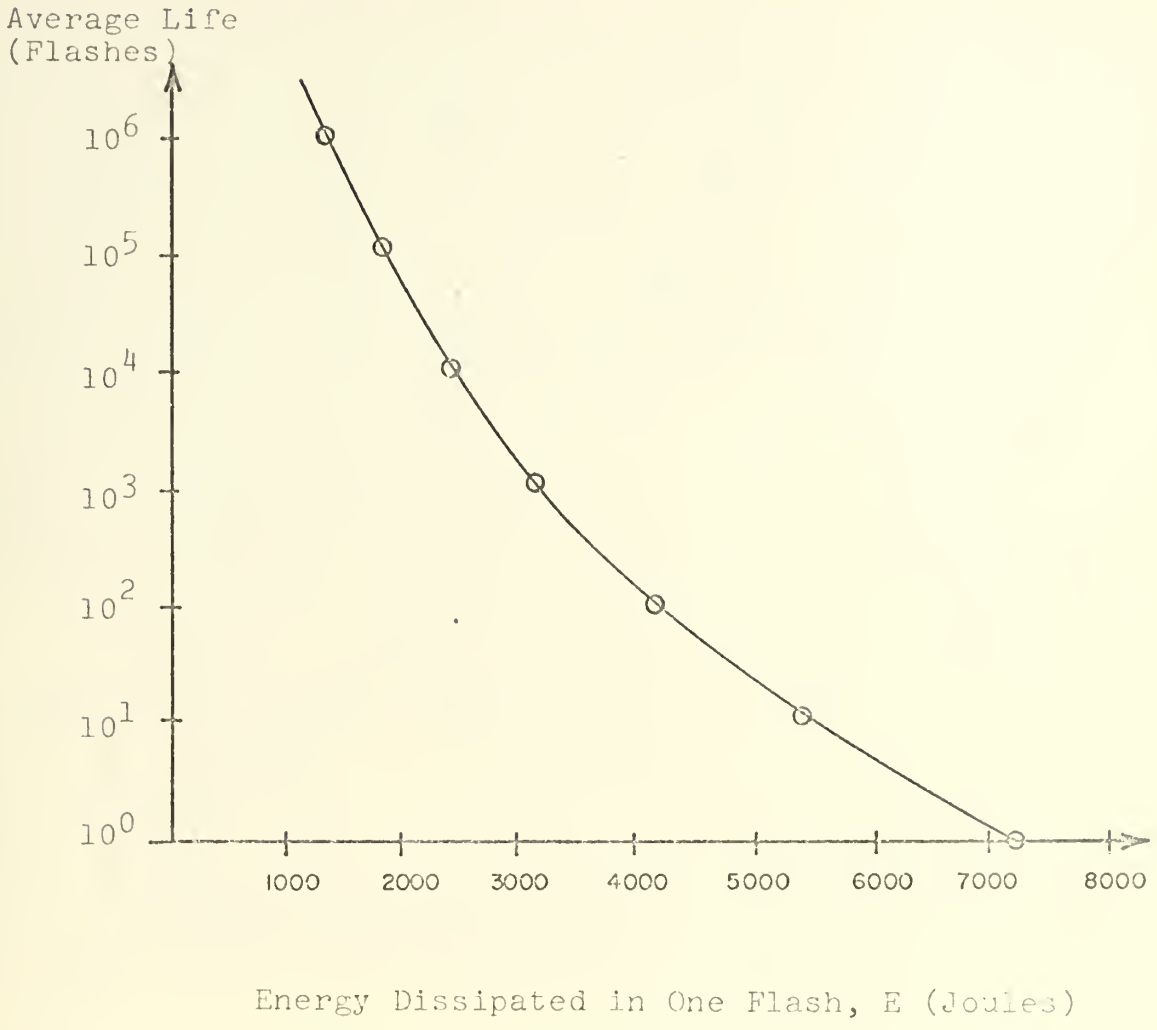

Figure 21. Lamp Lifetime vs. Energy Dissipated

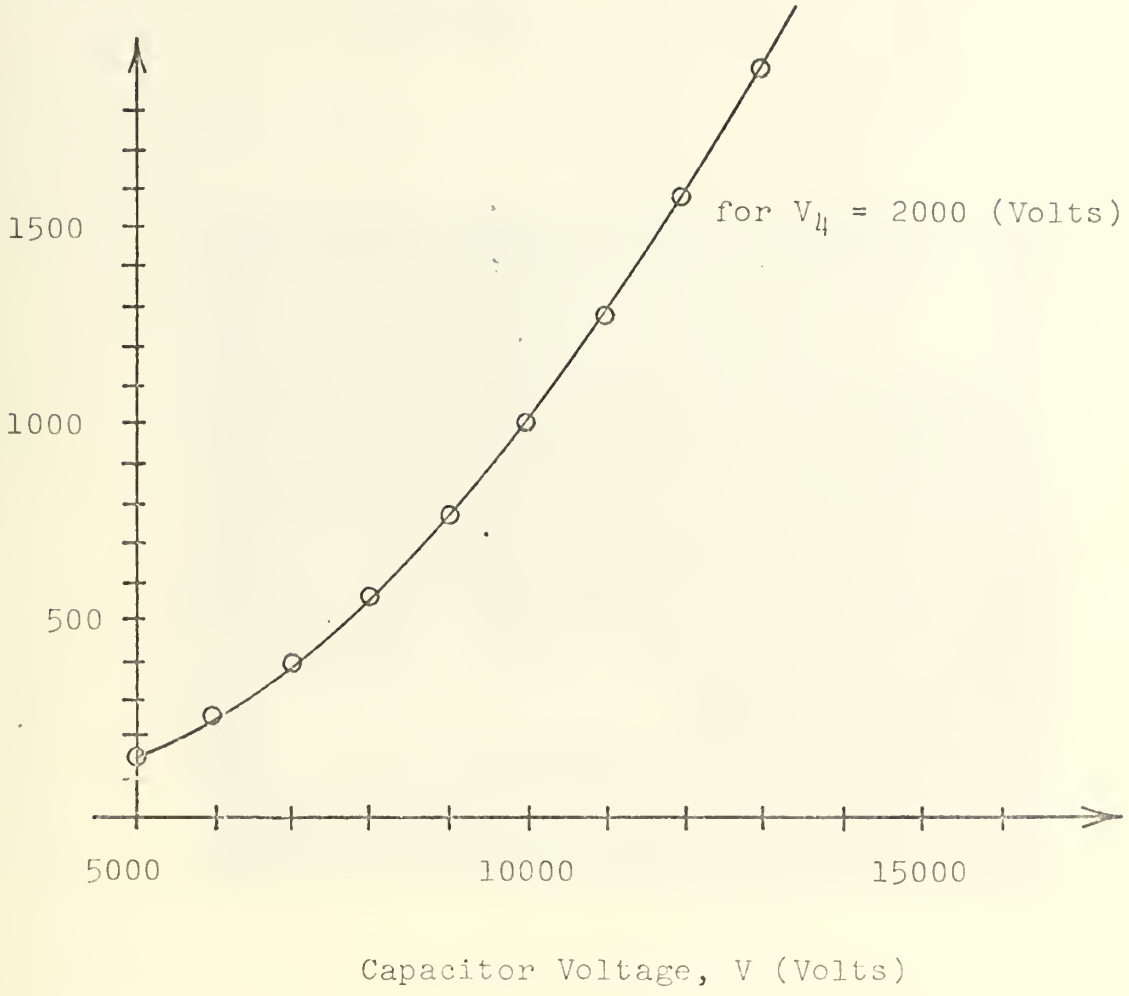

Figure 22. Flash Energy vs. Capacitor Voltage

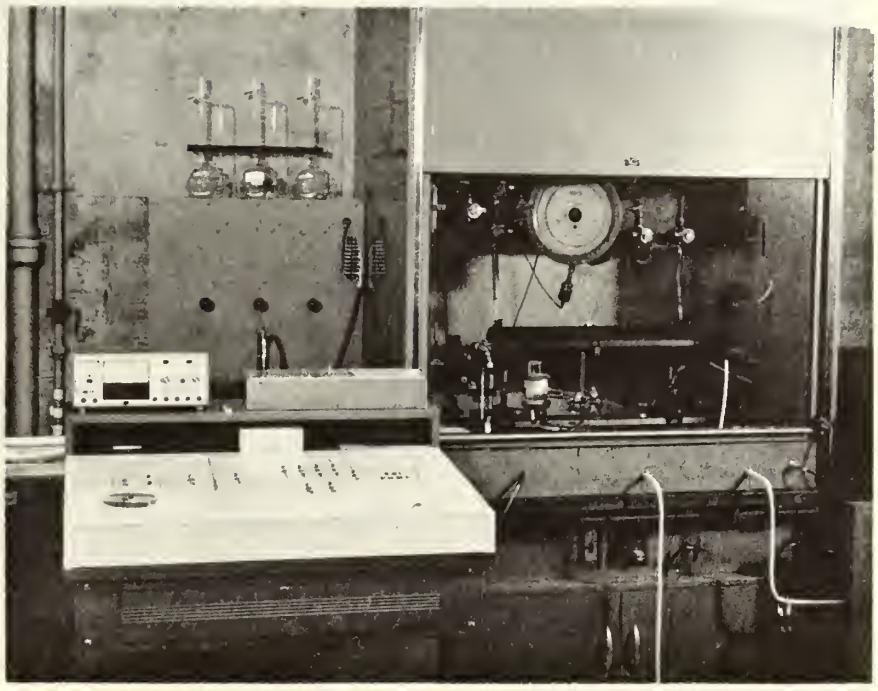

Figure 23. CO_2-HN_3 Laser and Control Panel

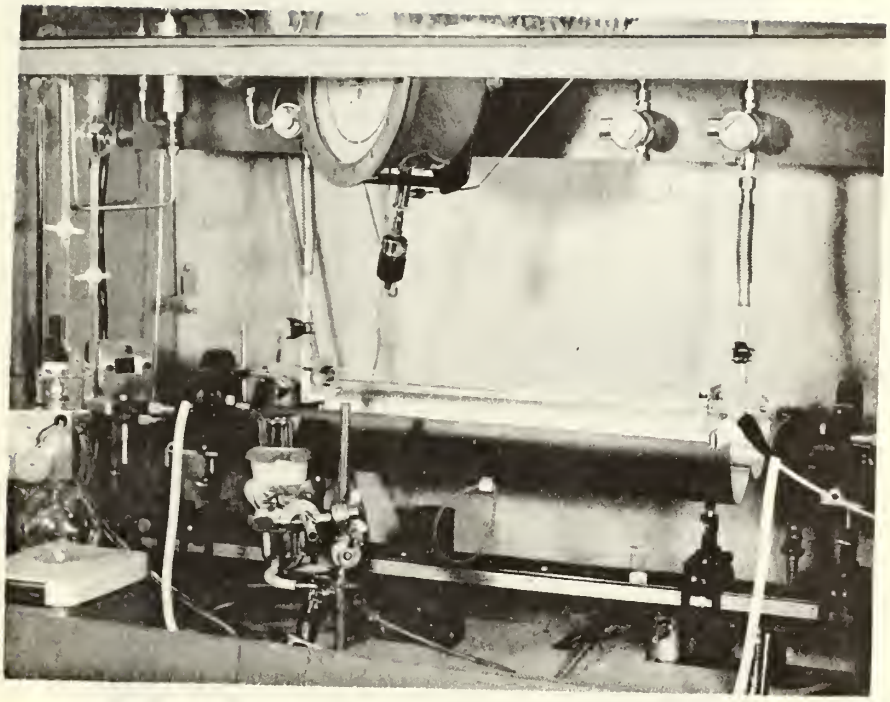

Figure 24. Optical Bench with Laser, Flashlamp, and IR Detector

Figure 25. HN_3 Generating Unit

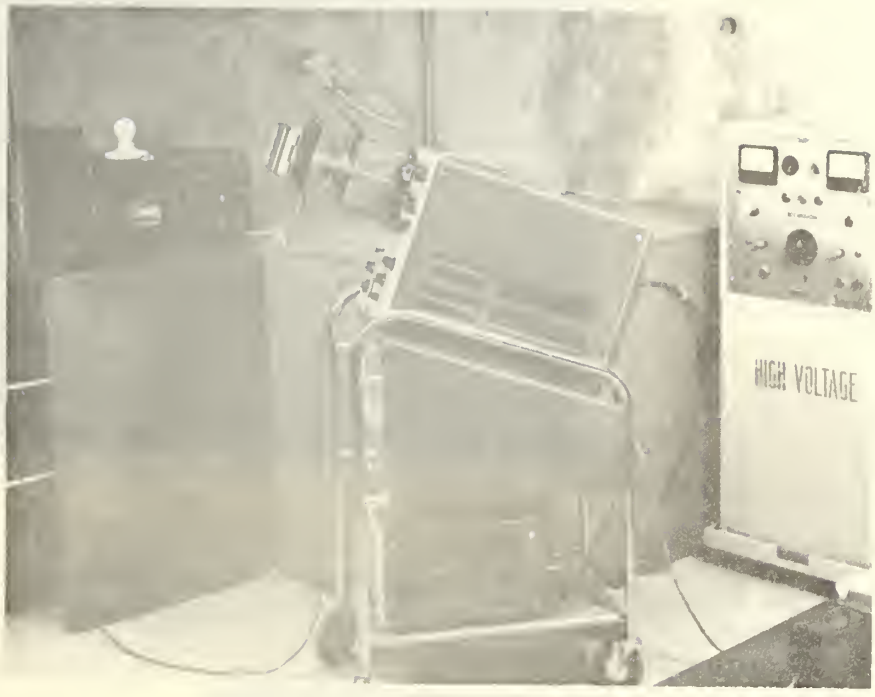

Figure 26. High Voltage Power Supply with Capacitor Bank, Trigger Unit, and Oscilloscope

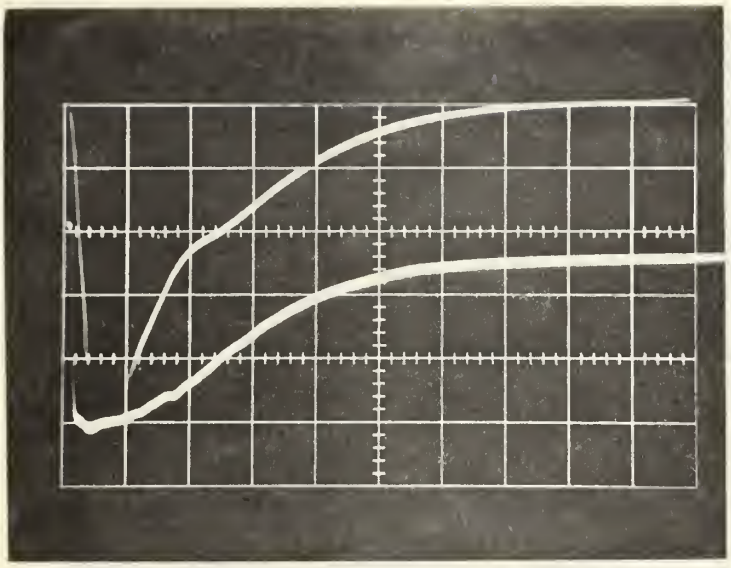

200 μsec/cm

Figure 27. Distorted Flashlamp Output Detected by Photomultiplier (upper trace) and IR Detector (lower trace). See also Chapter V, "Experimental Results."

50 μsec/cm

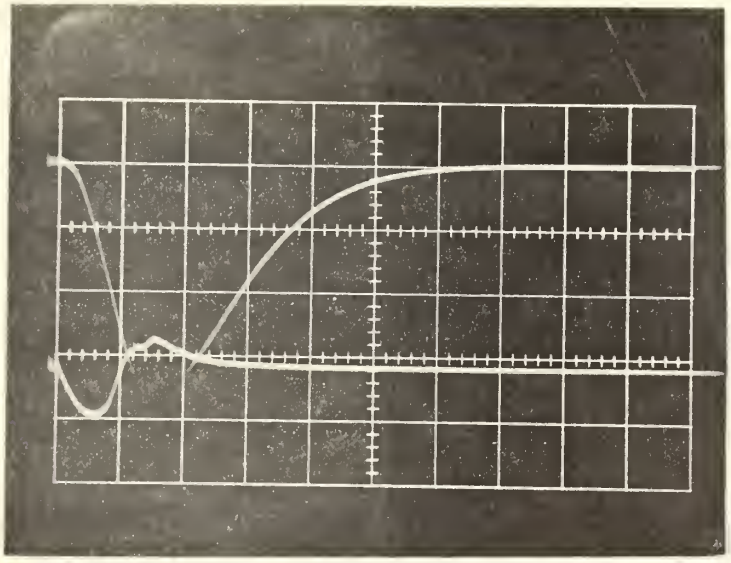

Figure 28. Flashlamp Output Detected by IR Detector (upper trace) and Discharge Current Pulse (lower trace). See also Chapter V, "Experimental Results."

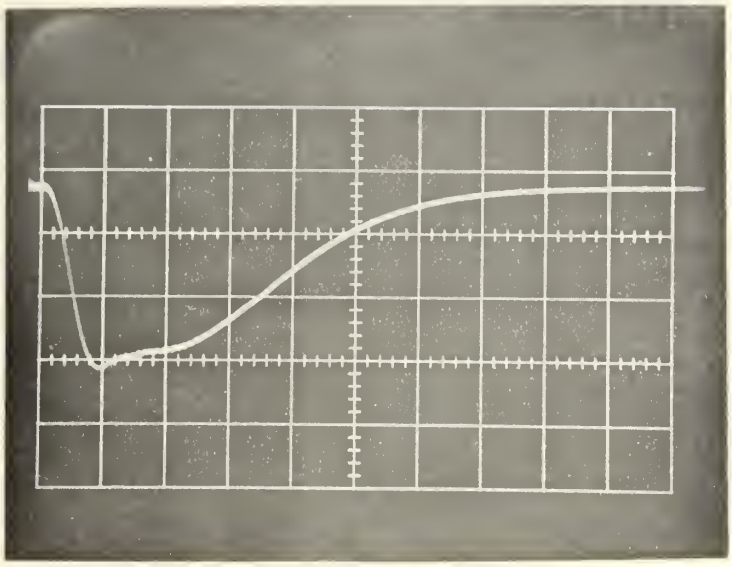

50 μsec/cm

Figure 29. Distorted Flashlamp Output Detected by IR Detector. See also Chapter V, "Experimental Results."

50 μsec/cm

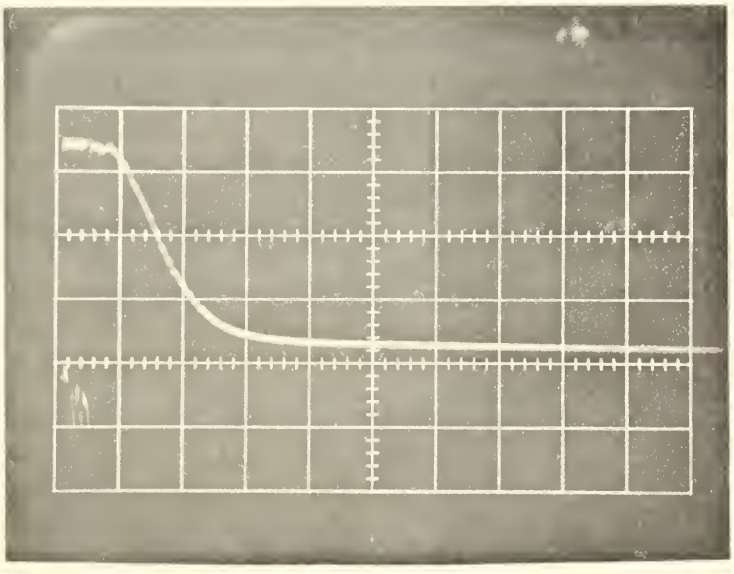

Figure 30. Capacitor Voltage During Discharge. See also Chapter V, "Experimental Results."

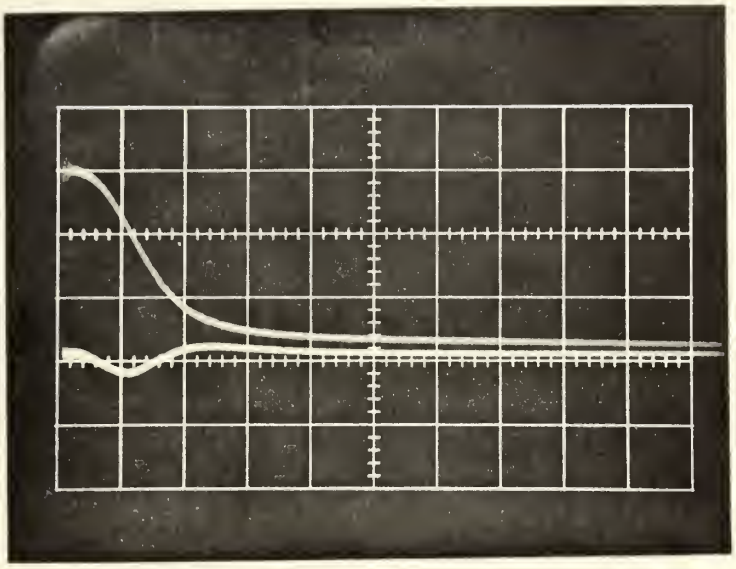

Figure 31. Capacitor Voltage (upper trace) and Discharge Current Pulse (lower trace). See also Chapter V, "Experimental Results."

BIBLIOGRAPHY

1. Garrett, C.G.B., Gas Lasers, McGraw-Hill, 1967.

2. Sanders, J.H., The Birth of the Laser, in Fishlock, D., A Guide to the Laser, American Elsevier Publishing Company, 1967.

3. Lengyel, B.A., Introduction to Laser Physics, Wiley, 1966.

4. Schulmann, R.D., Static Molecular Laser: Design, Construction and Operation; Including Investigation of the Dual Polarization Phenomenon, Master's Thesis, U.S. Naval Postgraduate School, Monterey, California, 1967.

5. Patel, C.K.N., et al., "CW Laser Action on the Rotational Transition $\Sigma_u^+ - \Sigma_g^+$ Vibrational Band of CO_2," Bulletin of the American Physical Society, v.9, p.500, 1964.

6. Patel, C.K.N., "Selective Excitation through Vibrational Energy Transfer and Optical Maser Action in N_2-CO_2," Physical Review Letters, v.13-21, 23 Nov. 1964.

7. Patel, C.K.N., "High Power Carbon Dioxide Lasers," Scientific American, Special edition, "Lasers and Light," Aug.1968.

8. Patel, C.K.N., "Continuous-Wave Laser Action on Vibrational Transitions of CO_2," Physical Review, v.136-5A, Nov.1964.

9. Gordiets, B.F., et al., "Kinetics of Physical Processes in CO_2 Lasers," Soviet Physics JETP, v.26-5, May 1968.

10. Basov, N.G. and Krokhin, O.N., "Population Inversion in a Discharge in a Mixture of Two Gases," Applied Optics, v.1-3, May 1962.

11 Anderson, J.D., "Time-Dependent Analysis of Population Inversions in an Expanding Gas," The Physics of Fluids, v.13-8, Aug.1970

12. Taylor, R.L. and Bitterman, S., "Survey of Vibrational Relaxation Data for Processes Important in the CO_2-N_2 Laser System," Review of Modern Physics, v.41-1, Jan.1969.

13. Moore, C.B., et al., "Vibrational Energy Transfer in CO_2 Laser," Journal of Chemical Physics, v.46-11, 1 June 1967.

14. Vincenti, W.G. and Kruger, C.H., Introduction to Physical Gas Dynamics, Wiley, 1965.

15. Corneil, P.H., The HCl Chemical Laser, Ph.D.Thesis, University of California, Berkeley, 1967.

16. Mitchell, A.C.G. and Zemansky, M.W., Resonance Radiation and Excited Atoms, Cambridge University Press, 1934.

17. U.S. Naval Ordnance Laboratory, NOLTR 70-198, Numerical Experiments Associated with Gas Dynamic Lasers, by J.D. Anderson, 24 Sept.1970.

18. Basov, N.G., et al., "Emission Stimulated by Explosion of HN_3 in CO_2," ZhETF Pis.Red., v.10-1,pp.5-8, 5 July 1969.

19. Dzhidzhoev, M.S., et al., "Creation of a Population Inversion in Polyatomic Molecules through the Energy of Chemical Reactions," Soviet Physics JETP, v.30-2, Feb.1970.

20. Cheo, P.K., and Cooper, H.G., "Gain Characteristics of CO_2 Laser Amplifiers at 10.6 Microns," IEEE Journal of Quantum Electronics, v.QE3-2, Feb.1967.

21. Cheo, P.K., "Relaxation of CO_2 Laser Levels by Collisions with Foreign Gases," IEEE Journal of Quantum Electronics, v.QE4-10, Oct.1968.

22. Christiansen, W.H. and Tsongas, G.A., "Gain Kinetics of High Pressure Gasdynamic Lasers," Aerospace Research Laboratory, University of Washington, Feb.1971.

23. Oral communication with Professor Rowell, Department of Chemistry, U.S. Naval Postgraduate School, Monterey, California.

24. Markiewicz, J.P. and Emmett, J.L., "Design of Flashlamp Driving Circuits," IEEE Journal of Quantum Electronics, v.QE2-11, Nov.1966.

25. Siegman, A.E., An Introduction to Lasers and Masers, Preliminary Edition, McGraw-Hill, 1968.

26. U.S. Naval Ordnance Laboratory, NOLTR 70-214, Vibrational Population Inversions within Normal Shock Waves in CO_2-N_2-He Mixtures, by J.D. Anderson, M.T. Madden, and C.H. Piper, 7 Oct.1970.

27. ILC Technical Publication, Preliminary Catalog, [illegible] Flashlamps, 1970.

INITIAL DISTRIBUTION LIST

		No. Copies
1.	Defense Documentation Center Cameron Station Alexandria, Virginia 22314	2
2.	Library, Code 0212 Naval Postgraduate School Monterey, California 93940	2
3.	Professor D.J. Collins, Code 57 Co Aeronautical Engineering Department Naval Postgraduate School Monterey, California 93940	2
4.	LCDR Gunther P. Schnez, FGN 53 Bonn - Bad Godesberg Axenfeldstr. 14, Germany	1
5.	Inspektion des Erziehungs-und Bildungswesens der Marine 294 Wilhelmshaven, Germany	1
6.	Dokumentationszentrale der Bundeswehr [See] 52 Bonn Friedrich Ebert Allee 34, Germany	1

Security Classification

DOCUMENT CONTROL DATA - R & D

(Security classification of title, body of abstract and indexing annotation must be entered when the overall report is classified)

1 ORIGINATING ACTIVITY (Corporate author)

Naval Postgraduate School
Monterey, California 93940

2a. REPORT SECURITY CLASSIFICATION

Unclassified

2b. GROUP

3 REPORT TITLE

The CO_2-HN_3 Laser: Design and Construction of a Molecular Laser Pumped by Photolysis of HN_3

4 DESCRIPTIVE NOTES (Type of report and, inclusive dates)

Master's Thesis; June 1971

5 AUTHOR(S) (First name, middle initial, last name)

Gunther P. Schnez

6. REPORT DATE	7a. TOTAL NO. OF PAGES	7b. NO. OF REFS
June 1971	94	27

8a. CONTRACT OR GRANT NO.	9a. ORIGINATOR'S REPORT NUMBER(S)
b. PROJECT NO	
c.	9b. OTHER REPORT NO(S) (Any other numbers that may be assigned this report)
d.	

10 DISTRIBUTION STATEMENT

Approved for public release; distribution unlimited.

11. SUPPLEMENTARY NOTES	12. SPONSORING MILITARY ACTIVITY
	Naval Postgraduate School Monterey, California 93940

13. ABSTRACT

A CO_2-HN_3 laser is designed and constructed. The use of hydrazoic acid, being highly explosive and toxic, requires a design where the gas handling and optical systems are located inside a fume hood with exhaust to the outside. The laser utilizes a pumping scheme where energy released by the photolysis of HN_3 is used to create a population inversion in CO_2.

The major highlights of the developmental work are: (1) design and fabrication of the laser tube and resonant cavity, (2) design, construction and operation of the HN_3 generating and gas filling systems, and (3) flashlamp discharge circuit design and development of the charging control system.

Operation of the laser is the subject of subsequent work with the system. Preliminary experiments and suggestions are included in this study. Furthermore the basic principles and equations governing the operation of a CO_2-HN_3 laser are derived.

DD FORM 1 NOV 65 1473 (PAGE 1)

S/N 0101-807-6811

Security Classification

A-31408

KEY WORDS	LINK A		LINK B		LINK C	
	ROLE	WT	ROLE	WT	ROLE	WT
O_2-HN_3 laser						
hotolysis						
esign						
onstruction						

128142

Thesis
S33795 Schnez
c.1

The CO_2-HN_3 laser: design and construction of a molecular laser pumped by photolysis of HN_3.